Mechanics of the Cochlea

Elizabeth S Olson[a,b], [a] Department of Otolaryngology, Head and Neck Surgery, Columbia University, New York, NY, United States; and [b] Department of Biomedical Engineering, Columbia University, New York, NY, United States

Abstract

Cochlear mechanics can be described in layers. The first layer is the classic passively tuned cochlear traveling wave. The traveling wave is present due to the fundamental mechanics of basilar membrane stiffness and fluid mass, and forms the physical substrate for cochlear processing. It is presented here in a teacherly way, to make its physical underpinning a familiar concept for those studying the cochlea. The second layer describes the effects that cell mechanics – the nonlinearity introduced by the saturation of mechanoelectric transduction, electromechanical transduction, the cochlear amplifier – have on the first layer. The recent ability to measure nanometer-scale motion responses within the sensory tissue has ignited new excitement in cochlear mechanics. Understanding how the electrical and mechanical responses work together to result in the marvelous mechanical processing of the living cochlea is the third layer of this article, and a work in process.

Introduction

Sounds, time-varying pressure waves, from all sources in the environment sum and enter the ear canal to form the auditory stimulus (**Fig. 1**). This pressure drives the flexible eardrum, which funnels the sound to the ossicles. Although some frequencies of sound are attenuated and others accentuated by the acoustics of the outer and middle ear, to first order the motion of the ossicles provides a good representation of the pressure stimulus at the eardrum – the middle ear transmits the sound stimulus to the inner ear with high fidelity (Olson, 1998; Nakajima et al., 2008; Dong et al., 2012). The final ossicle, the stapes, plunges in and out of the inner ear, transmitting the sound to the cochlea where its mechanical responses to the sound stimulus are finally converted to the electrical language of the brain.

The cochlea's sensory tissue, the organ of Corti complex (OCC = organ of Corti (OC) + basilar membrane (BM) + tectorial membrane (TM)), is a long narrow strip of tissue, surrounded on two sides by fluid chambers and coiling around a central cylinder. Within that central cylinder is the auditory nerve and its cell bodies forming the spiral ganglion (**Fig. 2**). In humans, the OCC is ~35 mm long and its width tapers from ~0.13 mm in the base to ~0.4 mm in the apex (Liu et al., 2015a; Raufer et al., 2019) – thus its aspect ratio is akin to that of a (tapering) meter stick. Audible sound is composed of pressure fluctuations with temporal periods ranging, for human hearing, from ~0.05 s down to ~50 μs (corresponding to 20 to 20000 Hz). In other mammals this range can be extended both upward and downward in frequency (West, 1985). The OCC vibrates in response to the pressure fluctuations, and the internal motions associated with this vibration stimulate the hair cells, the transducer cells of the cochlea. In the

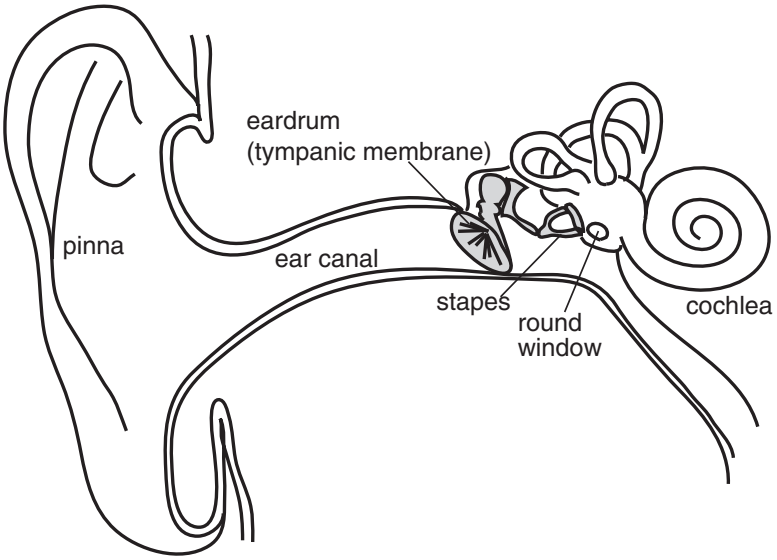

Figure 1 Sketch of the human ear (drawing courtesy of H. Heidi Nakajima).

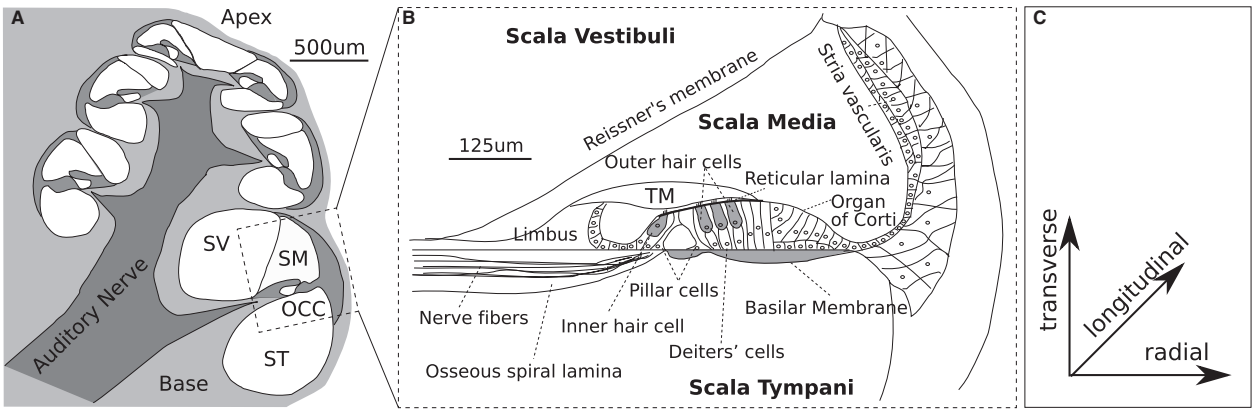

Figure 2 (A) Cross sectional sketch of the snail-shaped mammalian cochlea, with the fluid compartments scala tympani, vestibuli and media labeled ST, SV, and SM. The auditory nerve is central and branches to contact the sensory tissue of the organ of Corti complex (OCC). The fluid compartments and OCC spiral around the auditory nerve. (B) Boxed section in (A) expanded and labeled. The sensory tissue is comprised of the fibrous/gelatinous tectorial membrane (TM), the fibrous basilar membrane (BM) and the cellular structure they sandwich, the organ of Corti (OC). The BM, TM and OC together form the OCC. (C) Directions referred to in this chapter. Longitudinal is along the cochlear spiral.

human cochlea there are ∼15000 hair cells arranged in ∼3500 rows comprised of one inner and three (sometimes four) outer hair cells (Fig.2, Fig.10). The sound stimulus is represented in the pattern of motion along the length of the OCC.

In the eye, the counterpart to the OCC is the retina, where the visual stimulus is represented and converted to an electrical signal. Imagine a scene - a beach ball bouncing off to the left, a child moving toward the ball, snow sagging from a branch in the background and the bright beak of a crow peaking from foliage at the right. The reflected light from these different sources enters the eye as a sum. However, the sources all come from different directions, and because of the focusing of the eye's cornea and lens, images of the ball, child, snow and beak all have their own place on the retina - to some degree the visual periphery sorts the visual input by source. Similar to their reflected light, the sounds from these sources in the environment enter the outer ear as a sum. However, these sound sources are not represented at different locations along the ear's OCC – there is no physical mechanism available to the body to provide such a focusing. Instead, the summed sound, after traveling through the middle ear as a sum, is sorted in the inner ear by frequency. Generally, sound sources are composed of many frequencies and the different sources will share frequency components; the snow-plop, the child's yell, the caw of the crow, the ball-thump, all are represented by the patterns of motion they produce on the OCC, and these patterns will overlap. It is the brain's job to recompose the yell, thump, caw, plop from this pattern, and the ear's job to represent the patterns as clearly as possible. Although a separate topic than cochlear mechanics, binaural processing by the brain, and directional-dependent filtering of sound source frequencies by the outer and middle ear also play roles in the discrimination of sound sources (Ashida and Carr, 2011; Colburn et al., 1996; Pecka, 2020).

Cochlear mechanics is the story of the mechanical and electromechanical processes that produce the cochlea's frequency sorting. The understanding of cochlear mechanics proceeds in layers. The first layer is the passive tuning based in the cochlear traveling wave.

This layer contains basic descriptions of the OCC anatomy and of the sound-induced motions of the sensory tissue's BM. Because of the centrality of the traveling wave, this part of the article contains a simple traveling wave model. The second layer begins with post - 1970 observations of the sound-induced motions of the BM, including the discovery of nonlinearity and physiologically-based enhancement of mechanical tuning – cochlear activity, also referred to as the cochlear amplifier. In this layer the feedback of hair cell mechanics to the sound-induced motions becomes apparent, in particular outer hair cell (OHC) electromechanics and the saturating nonlinearity of mechanoelectric transduction (MET). Because of the centrality of nonlinearity to cochlear mechanics, this part of the article includes a derivation of the two-state Boltzmann distribution as applied to the MET channel. Layer 3 is the modern attempt to understand *how* cochlear amplification works. Following the observations of cochlear activity and nonlinearity, understanding how cell-based micromechanics coupled into the traveling wave became a focus of exploration. Genetic mouse models with mutations targeted to the TM emphasized the influence of the TM to the micromechanical processing. Exciting new information about cochlear mechanics has come from optical coherence tomography (OCT) based observations of sound-induced motions deep within the OCC. The OCT-based observations span layers 2 and 3, and to first order, they reinforce that the cochlear traveling wave is the underlying substrate of cochlear mechanical processing. As the OCT measurements mature and become more spatially resolved, the understanding of cochlear mechanical processing will advance further.

There are good reviews of cochlear mechanics in the literature and several are noted here: The 2001 review of cochlear mechanics (Robles and Ruggero, 2001) discussed experimental observations of cochlear amplification and cochlear nonlinearity, and emphasized macromechanical measurements of BM motion. A recent review of cochlear amplification included a description of TM mechanics, and discussed explorations into the micromechanical basis for the cochlear amplifier (Gummer et al., 2017). A short review that was a tribute to von Békésy updated aspects of cochlear mechanics that were central to Békésy's pioneering work (Olson et al., 2012). A recent review and tutorial on cochlear mechanics and modeling is in (Reichenbach and Hudspeth, 2014). The 1980s teacherly articles (de Boer, 1980) (de Boer, 1984) and a short, lucid tutorial (Kolston, 2000) outline basics of cochlear mechanics and modeling.

Some History

In the mid 1850s, Retzius, Testut and others drew the anatomy of the OCC (**Fig. 3**A and B). These early drawings depicted the basic structure of hair cells, pillar cells, supporting cells, TM and BM, and emphasized the prominent radial anatomy of the fibers of the BM. The cochlea's anatomy had already been compared to a harp-like musical instrument by the time Helmholtz applied the decades-old theory of Fourier analysis and proposed that the cochlea performed a mechanical Fourier analysis, by means of mechanical resonators arranged tonotopically along the cochlea (shorter and stiffer at base = high frequency, longer and more compliant at apex = low frequency) (Helmholtz, 1885). (**Fig. 2**A identifies the base and the apex in the mammalian cochlea.) A history of cochlear tonotopicity, going back to ancient Greece, was recently written (Ruben, 2020). The "place theory of hearing" is now well established although the explanation for it has evolved.

In the 1920s−1940s Békésy made his historic observations of sound-induced cochlear motions and observed the cochlear traveling wave (Békésy, 1960). He experimented on everyday objects to understand the basis for the wave, and found that virtually all deformable systems showed waves at some frequency of stimulation; he noted that he could not publish these findings in a physics journal because to a physicist this was obvious (Békésy, 1961). Békésy's traveling wave responses showed a mild peak at a location that was in the base of the cochlea for high frequency stimulation and further apical for low frequency stimulation. This "tonotopic" tuning is the major basis for the cochlea's frequency sorting. For sound frequencies up to several kHz, frequency sorting is also provided by phase-locked action potentials in auditory neurons (Verschooten et al., 2019).

Even before Békésy observed the cochlear traveling wave, Helmoltz's local resonance theory had been supplanted by dynamical theories that recognized that the radial fibers of the BM were coupled by the surrounding fluid, and thus they would not operate as independent resonators. Before Békésy's observations (Wegel and Lane, 1924) and in earnest following them, traveling wave models were developed (Wever, 1962). These models were able to produce the passive mechanical responses of the cochlea but were not able to account for the sharp tuning that was known to exist in auditory nerve fibers. The pioneering measurements of Rhode and colleagues (Rhode, 1971), showing the enhanced, nonlinear tuning of the BM in healthy cochleae at low-to-moderate sound pressure level, shifted the puzzle. The new measurements ultimately showed that mechanical responses were as sharply tuned in frequency as auditory nerve responses (Naryan et al., 1998), and now cochlear models needed to catch up. The idea for an active cochlea had been proposed as a concept (Gold and Pumphrey, 1948). Traveling wave models incorporating this concept were able to produce realistic tuning, with activity in the form of a negative damping (Neely and Kim, 1986). In 1985 Brownell and colleagues discovered OHC electromotility (Brownell et al., 1985), and in 2000 Dallos's group cloned the OHC's electromechanical protein, which they named Prestin (Zheng et al., 2000). These were the seminal discoveries forming the modern understanding of cochlear mechanics: the cochlea is active and its activity lies in OHCs.

Layer 1: The Physics of Passive Cochlear Mechanics

The first layer will be presented as a teaching/learning tool, with the physics behind the cochlear traveling wave presented simply and as stripped of extraneous details as possible, to convey the essence of the cochlear traveling wave and to provide a simple explorable cochlear model.

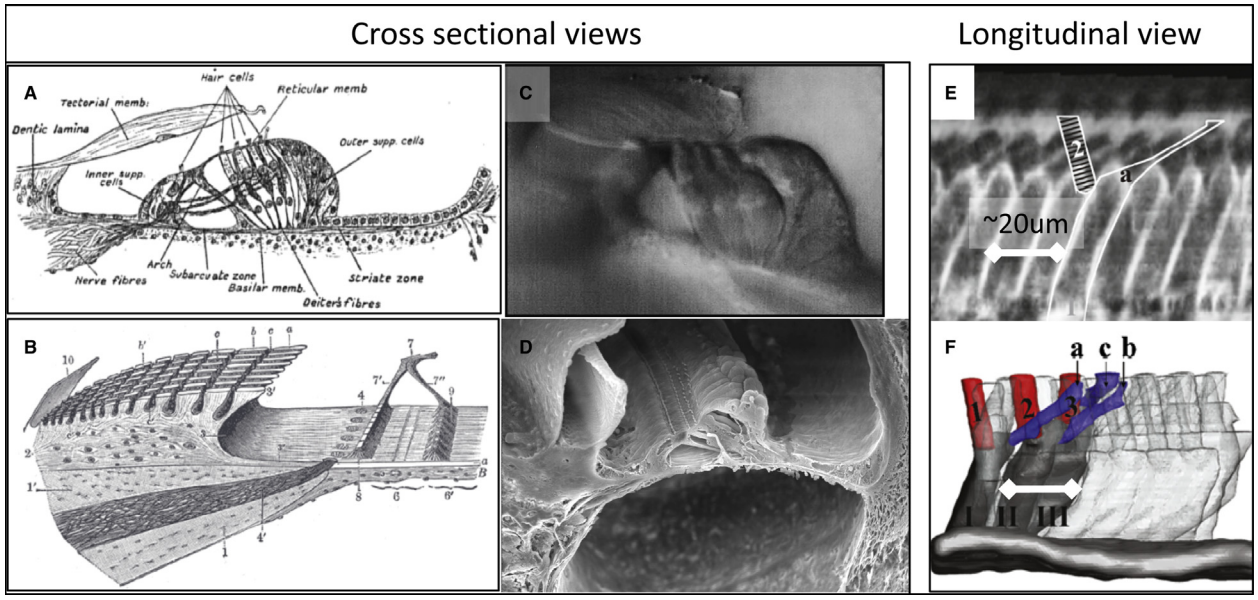

Figure 3 A and B: Early anatomical drawings of the cochlear cross section. (A) From Retzius, Das Gehörorgan der Wirbeltiere, 1884, Stockholm. (B) From Testut, in a textbook of physiology for medical students and physicians (p.403) by WH Howell, 1910, W.B. Saunders company, Philadelphia, London. (C) Unfixed cochlea from gerbil shows the natural position of the TM atop the hair cells. (Image has been transposed left-to-right from the original to conform to A,B,D) (Edge et al., 1998). (D) Electron microscopic image from guinea pig gives a sense of the large fluid spaces surrounding the OCC. Courtesy of Bechara Kachar (NIH/NIDCD). In A,B,D, fixation lifted the TM from its natural position. For approximate lengths in A-D, consult scale bar in **Fig. 2**. (E) Longitudinal view from unfixed mouse cochlea and corresponding computed reconstruction in F shows the striking longitudinal tilt of Deiters cells' processes (purple in F, labeled a in E) and to a lesser degree of OHCs (red in F, labeled 2 in E). The base is to the left, the apex to the right (Soons et al., 2015).

Measurements of the Cochlear Traveling Wave

While Békésy and a few modern experimentalists (Ren, 2002; Fisher et al., 2012) managed to measure an extent of the cochlear traveling wave's spatial pattern for a single frequency of stimulation, most scientists observe at one spatial location and at many frequencies, and from the amplitude of the response, and the phase of the response relative to a reference such as ear canal pressure or stapes motion, deduce the cochlear traveling wave. An example of BM motion data upon pure tone stimulation from the base of the chinchilla cochlea (slightly smoothed from the original) is in **Fig. 4**A and B (Rhode, 2007a). **Fig.4C** shows an idealized view of the underlying spatial waveforms that gave rise to the multi-cycle phase excursion of **Fig.4B**. Useful as data like that of **Fig.4** A and B is, mathematical cochlear models predict the cochlea's spatial response and need spatial response data to be developed and evaluated. Fortunately, we are able to use data like that in **Fig. 4**A and B to construct the spatial response – to quantitatively construct the response curves in **Fig.4C**. This ability is based on the concept of "scaling symmetry."

The Concept of Scaling Symmetry

The concept of scaling symmetry was based on the observation that BM motion frequency responses (data as in **Fig. 4**A and B) have a characteristic shape, which is maintained at different locations along the BM; the peak frequency shifted to lower frequencies for more apical measurement locations, but the tuning and phase excursion were constant features (Zweig, 1991). This constant tuning shape is even more apparent in auditory nerve (AN) tuning curves, because, unlike the BM frequency responses that were measured only close to the base, AN responses could be measured from locations all along the cochlea. An example is in **Fig. 5** where auditory nerve frequency tuning curves from fibers scanning characteristic frequencies from 4.8 to 19 kHz are shown. The curves are plotted with the x axis frequency/characteristic-frequency, and lie nearly on top of each other, showing the concept of scaling symmetry. Departure from ideal scaling symmetry becomes more pronounced at lower frequencies, as will be discussed in Section "**Apical/Basal Differences**."

The concept of scaling symmetry allows us to construct a spatial response from (i) a frequency response at one location and (ii) the species-specific map of characteristic frequency versus location. This map, termed the "tonotopic map" has been detailed for several species (Greenwood, 1990). The tonotopic map was typically determined by staining AN fibers so that their location in the cochlea could be identified, following a neurophysiological measurement to determine the characteristic frequency of the fiber (Greenwood, 1990). Tonotopic maps have also been determined with local measurements of cochlear microphonic (the extracellular voltage response of hair cells) (Schmiedt and Zwislocki, 1977) and from localized damage from powerful tones

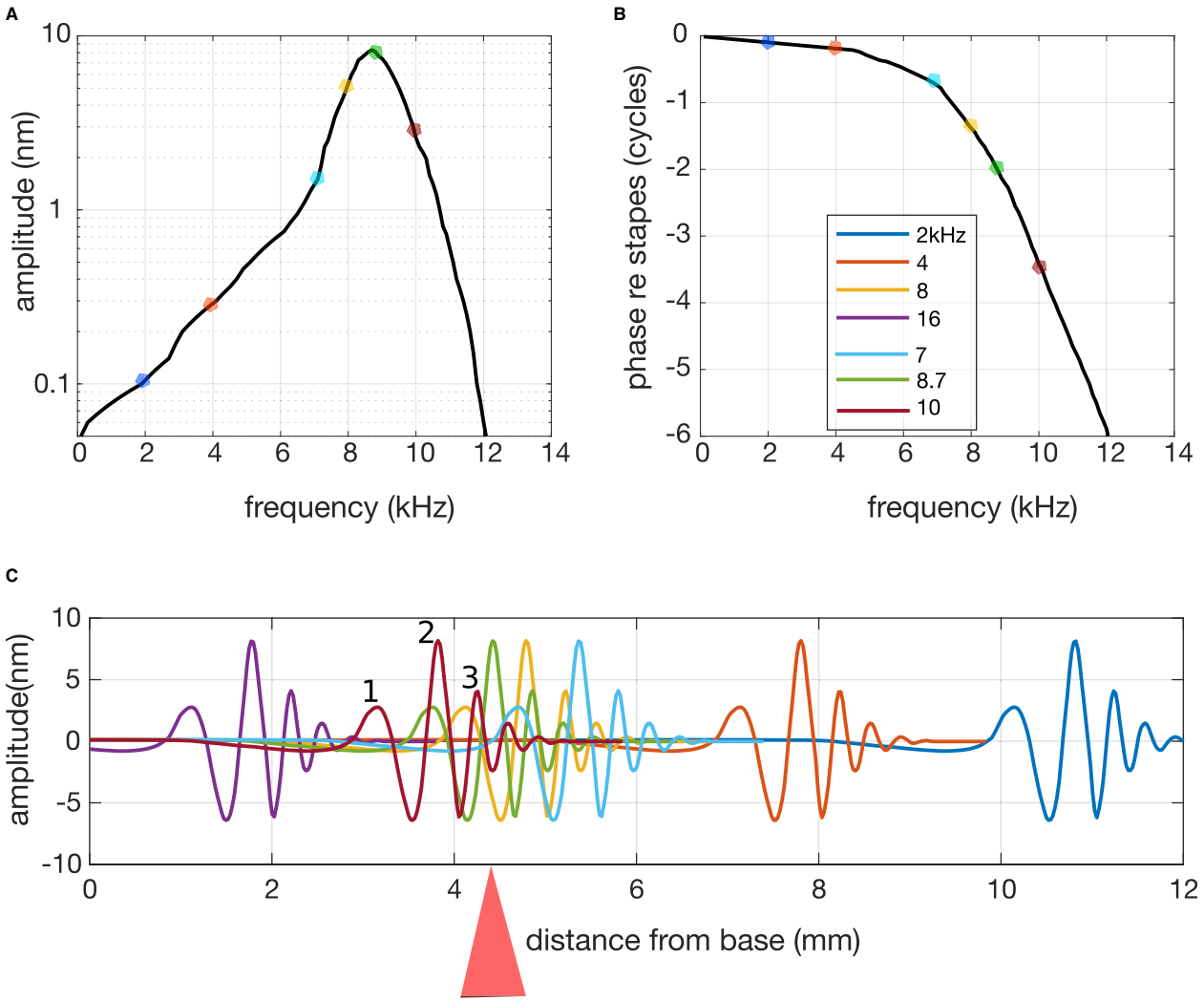

Figure 4 A and B) Amplitude and phase of an exemplary BM motion response. The observation point in A and B is indicated by the red arrowhead in C. Responses at seven frequencies are shown and color coded in C; in A and B these frequencies are the colored dots. The multi-cycle phase excursion in B is related to the underlying traveling wave responses at the frequencies color-coded in B. The numbers 1 2 3 above the 10 kHz wave are there to clearly indicate that >3 cycles have passed prior to the measurement location. C is an idealized view in which the wave pattern is the same for every stimulus frequency, thus showing perfect "scaling symmetry." In sections on glides and apical/basal differences a more realistic view will be discussed.

(Eldredge et al., 1981). The relationship between longitudinal distance from the apex and the characteristic frequency is ~exponential (Greenwood, 1990). An example of a tonotopic map from gerbil is plotted in Fig. 6.

The steps for finding the spatial response are: (1) Measure the mechanical frequency response (for example, BM motion or pressure at the BM) at one location, and find the frequency of the peak at low SPL; call this peak frequency BF. (Note: typically "best frequency" (BF) is used for mechanical peak frequency and "characteristic frequency" CF is used for auditory nerve threshold responses. At low SPL, BF = CF.) (2) Write this data in a table with the first column f, the second column f/BF and third and fourth columns the measured response magnitude and phase, R_{amp}, R_{phase} (phase relative to the input to the cochlea, for example stapes motion). A frequency response plot and corresponding data table are on the left side of Fig. 6, with the frequency shown in kHz and also normalized as frequency/BF. This will serve as a "look-up" table. Smoothed data of the pressure close to the BM is used for the example of Fig. 6. (3) Look in the literature to find the tonotopic map, CF(x), for your species. Write it in a table with x = distance from the base in the first column and CF(x) in the second column. The map for gerbil, whose sensory tissue is ~11 mm when uncoiled (Plassman et al., 1987), is in the first two columns of the right side table of Fig. 6. (4) Decide what frequency you want to see the spatial response for. Call this f0 and divide it by CF(x). This is a new column in the right-side table. (5) Use the look-up table to find R_{amp} and R_{phase} for f0/CF(x). With these values, fill in two columns on the right side. These are the amplitude and phase of the spatial response for stimulus frequency f0. In Fig. 6 example table entries are given for two f0 frequencies, 10 kHz and 1 kHz. Working with the look-up table will involve interpolation because the f/BF and f/CF values are different in the two tables. The interpolation can be implemented using matlab's "interp1" function. The useful range of the look-up table is limited

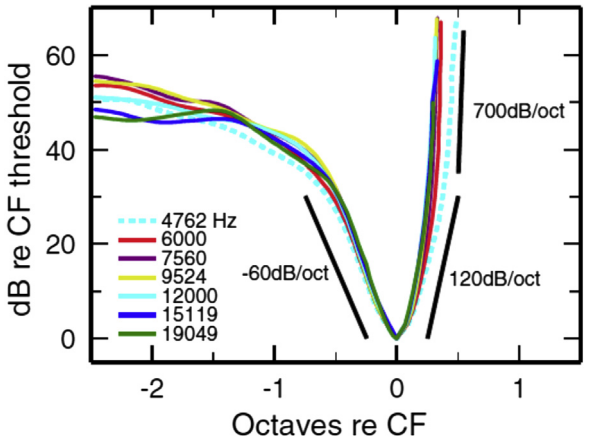

Figure 5 Auditory nerve threshold tuning curves from chinchilla. The sound pressure level (dB SPL) needed to elicit a "threshold" response in the nerve is plotted on the y axis versus frequency on the x axis. The frequency axis is normalized by CF, and the SPL axis is normalized to the level at CF threshold. Over a wide range of CF frequency (4.8–19 kHz) the curves essentially overlie (Temchin et al., 2008).

by the frequency range over which data were taken. Thus the spatial response at any chosen f0 will not extend through the entire cochlea. In the table at the right of Fig. 6 the yellow shading shows the spatial locations for which interpolation was possible for the two example frequencies. To the left of the right-side table spatial responses for 10 kHz, 1 kHz and several other frequencies are plotted. Because of departures from scaling symmetry in the real cochlea, the generated spatial responses are most reasonable for frequencies around the BF of the measured response, which was ~20 kHz (left side of Fig. 6). Thus, the 10, 20 and 40 kHz responses on the right side are the most accurately estimated spatial responses.

Passive Cochlear Models: Physics of the Cochlear Traveling Wave

To construct the cochlear sensing system, the body had to work with the available materials of biology: collagen, keratin, elastin, gel-forming glycoprotein/structural protein combinations and lipid-spanning channel proteins. The cochlea has been inventive, for example by making an energy consuming mechanical system whose heavily vascularized energy source, the stria vascularis, is spatially separated from the moving mechanical parts (Fig. 2B); by finding/modifying proteins that can open and close and exert forces on adjacent structures at frequencies up to ~0.1 MHz. The compliance and density of very standard biological materials – collagen and saline – provide the ingredients for the first level of frequency sorting along the OCC– what we call the passive tuning of the BM's traveling wave response. In this section we introduce the physics behind the cochlear traveling wave.

In a wave, a key quantity is wave speed. For example, in a string wave the speed is $c = \sqrt{\tau/\mu}$, where τ is tension in $N(\text{units}: N = kg\ m/s^2)$ and μ is linear density (kg/m). In a sound wave the speed is $c = \sqrt{B/\rho}$, where B is the bulk modulus of the medium in Pa (N/m^2) and ρ is density of the medium (kg/m^3). Once the wave speed is known, and a frequency f is prescribed, the wavelength $\lambda = c/f$. The function describing a wave moving in the $+x$ direction is $Acos(kx - \omega t)$ where $k = 2\pi/\lambda$ and $\omega = 2\pi f$, so $c = \omega/k$. A is the amplitude and in general will be a function of x,$A(x)$. $(kx - \omega t)$ is the phase of the wavefunction. A snapshot of the wave (t fixed) shows the wave undulating with a full wavelength every time kx goes through 2π radians. A distensible material providing restoring force (due to compliance, tension or gravity for example) and inertia are the ingredients for a mechanical wave. In the cochlea, wave speed is proportional to a ratio of BM stiffness (normalized to area, with units Pa/m), and the "effective" mass of the cochlear fluid.

In the description above k and thus λ were presented as constants, but it is clear from Fig. 4 that λ and thus k vary longitudinally. When developing a cochlear traveling wave model the relationship between k, termed "wavenumber", and ω is first determined. From that relationship, the phase of the wave function can be written, wave speed can be determined and more. We'll show this below for the simplest cochlear model, the 2-dimensional (2D) short-wave model (descriptively referred to by Egbert de Boer as the "wall-to-wall carpet" model) (Fig. 7B).

BM stiffness has been found with point stiffness measurements, with simultaneous measurements of pressure and displacement, and with a combination of motion measurements and cochlear modeling; it has been derived based on tissue properties and geometry (more on this in Section "**Back to the Traveling Wave**"). (Side note - for this simple model we make no distinction between BM stiffness and OCC stiffness.) However, in many cochlear models (including the 2D model developed below (Siebert, 1974)), in order to reduce complexity and parameters, the BM stiffness is only loosely based on direct measurements of physical properties; rather, its size and longitudinal variation is found such that the model produces the known tonotopic (place:frequency) map. This is typically an exponential function, with stiffness decreasing exponentially from the base to the apex.

The effective fluid mass/area is equal to fluid density (ρ) multiplied by fluid height. The fluid height is not a simple anatomical height, it refers to the effective height of fluid that moves with the wave, and it is found using fluid mechanical equations. In a 3D cochlear model the fluid height depends on the cross-sectional dimensions of the fluid chambers and the wavenumber k. In the 2D

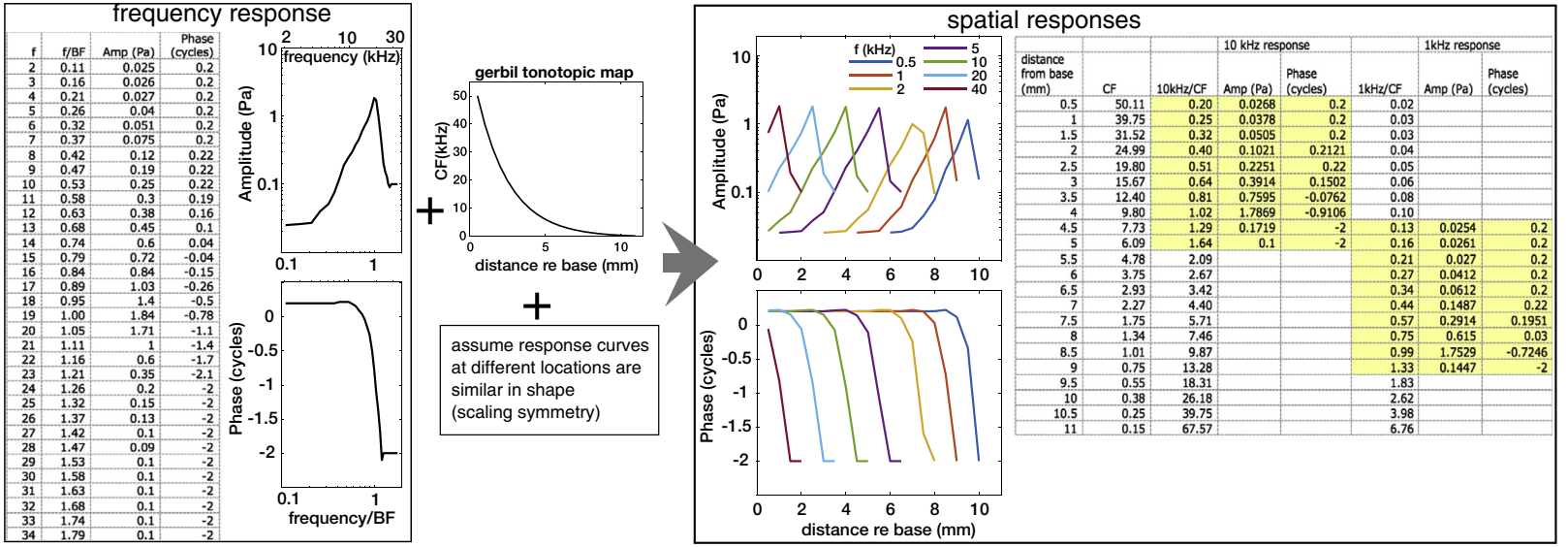

f	f/BF	Amp (Pa)	Phase (cycles)
2	0.11	0.025	0.2
3	0.16	0.026	0.2
4	0.21	0.027	0.2
5	0.26	0.04	0.2
6	0.32	0.051	0.2
7	0.37	0.075	0.2
8	0.42	0.12	0.22
9	0.47	0.19	0.22
10	0.53	0.25	0.22
11	0.58	0.3	0.19
12	0.63	0.38	0.16
13	0.68	0.45	0.1
14	0.74	0.6	0.04
15	0.79	0.72	-0.04
16	0.84	0.84	-0.15
17	0.89	1.03	-0.26
18	0.95	1.4	-0.5
19	1.00	1.84	-0.78
20	1.05	1.71	-1.1
21	1.11	1	-1.4
22	1.16	0.6	-1.7
23	1.21	0.35	-2.1
24	1.26	0.2	-2
25	1.32	0.15	-2
26	1.37	0.13	-2
27	1.42	0.1	-2
28	1.47	0.09	-2
29	1.53	0.1	-2
30	1.58	0.1	-2
31	1.63	0.1	-2
32	1.68	0.1	-2
33	1.74	0.1	-2
34	1.79	0.1	-2

distance from base (mm)	CF	10kHz/CF	10 kHz response Amp (Pa)	10 kHz response Phase (cycles)	1kHz/CF	1kHz response Amp (Pa)	1kHz response Phase (cycles)
0.5	50.11	0.20	0.0268	0.2	0.02		
1	39.75	0.25	0.0378	0.2	0.03		
1.5	31.52	0.32	0.0505	0.2	0.03		
2	24.99	0.40	0.1021	0.2121	0.04		
2.5	19.80	0.51	0.2251	0.22	0.05		
3	15.67	0.64	0.3914	0.1502	0.06		
3.5	12.40	0.81	0.7595	-0.0762	0.08		
4	9.80	1.02	1.7869	-0.9106	0.10		
4.5	7.73	1.29	0.1719	-2	0.13	0.0254	0.2
5	6.09	1.64	0.1	-2	0.16	0.0261	0.2
5.5	4.78	2.09			0.21	0.027	0.2
6	3.75	2.67			0.27	0.0412	0.2
6.5	2.93	3.42			0.34	0.0612	0.2
7	2.27	4.40			0.44	0.1487	0.22
7.5	1.75	5.71			0.57	0.2914	0.1951
8	1.34	7.46			0.75	0.615	0.03
8.5	1.01	9.87			0.99	1.7529	-0.7246
9	0.75	13.28			1.33	0.1447	-2
9.5	0.55	18.31			1.83		
10	0.38	26.18			2.62		
10.5	0.25	39.75			3.98		
11	0.15	67.57			6.76		

Figure 6 Scheme for using frequency response data (responses measured at one location to many frequencies) to estimate spatial response (response at one frequency, along the cochlea). See text for further explanation.

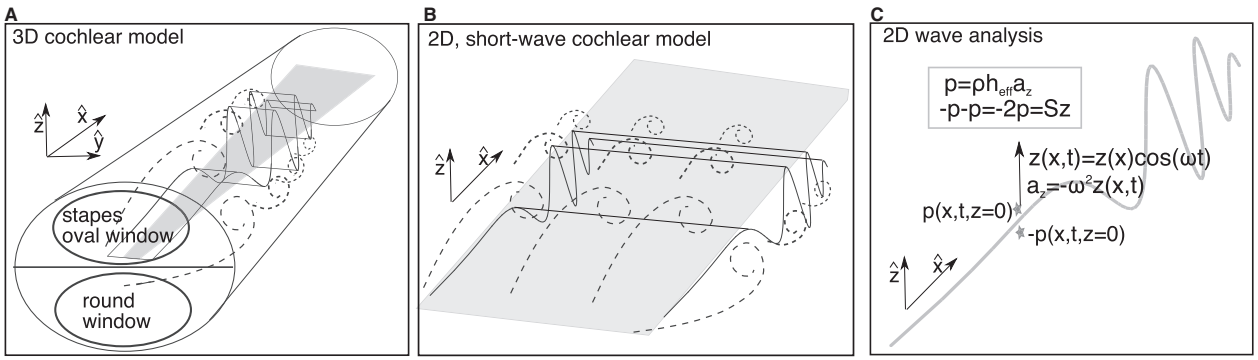

Figure 7 A) In a 3D cochlear model the fluid chambers are typically rectangular or oval. The longitudinal extent of the cochlea is uncoiled. Scala media and vestibuli are merged into one chamber (upper), which is identical to the chamber of scala tympani (lower). This is a symmetric cochlear model. (B) In a 2D short wave model, the fluid chambers are infinite in the z direction and no variations occur in the y direction. The dashed lines in A and B are cartoons to indicate that the fluid moves in circles (Lighthill, 1981). (C) The 2D model allows for a very simplified analysis, governed by the two boxed equations. The cochlear fluid is considered inviscid and incompressible. See text for further explanation.

short-wave model, the fluid height is found to be very simple: $h_{eff} = 1/k$ (Siebert, 1974). (A brief derivation of this result is in appendix B of (deLaRochefoucauld and Olson, 2007).) This simple result makes intuitive sense: the amount of fluid that sloshes back and forth with the motion of the wave is shorter for shorter λ, so h_{eff} is proportional to λ and inversely proportional to k. Fluid mass is the only mass in our simple model. Including mass in the OCC has the effect of reducing its stiffness in a frequency dependent manner, and allows for the possibility of local resonance. Including significant mass in the OCC may be incorrect physically if the cells and TM are very fluid (Siebert, 1974; Taber and Steele, 1981), and OCC mass is not needed to predict the passive BM tuning and traveling wave. The question of OCC mass and local resonance has been explored in models and experiments (Lighthill, 1981; deLaRochefoucauld and Olson, 2007; Eze and Olson, 2011; Steele and Taber, 1979a).

Moving forward: At every location along the longitudinal extent of the BM, the same pressure, at the BM, drives the displacement of the fluid mass and the displacement of the BM (Fig. 7C). The pressure at the BM varies in the x direction as a wave, and in the analysis here the symbol p represents pressure at the BM. (Pressure varies in the z direction (Olson, 1999; Olson, 2013), and that variation is included in the 2D model via h_{eff}, but the pressure that is considered here is the pressure at the BM.)

$$p = p_{amp}(x)cos(kx - \omega t) \tag{1}$$

As noted above, k varies with x, and the form of that dependence will be determined below. p_{amp} is the amplitude of the pressure wave.

Consider the pressure at the BM at any x location in Fig. 7C. Looking up the pressure driving the fluid motion is:

$$p = \rho h_{eff} a_z = \rho a_z / k \tag{2}$$

a_z is the vertical acceleration of the fluid. Eq. (2) is a dynamic correlate of the familiar static pressure that one feels diving under the surface of a pool, $p = \rho hg$, where g is the acceleration due to gravity.

Looking down in Fig. 7C, this same pressure is driving the motion of the BM, whose stiffness is defined as S:

$$2p = -Sz \tag{3}$$

This is the familiar Hooke's law, "Force = spring-constant times displacement", normalized to area, and using S for the spring constant/area. The factor of 2 represents the fact that the pressure driving BM motion is the pressure difference across the BM, which is twice the pressure on one side in symmetric cochlear models (gray stars in Fig. 7C identify the pressures going into the difference). Noting that $a_z = -\omega^2 z$ (easily seen by recognizing that $a_z = d^2z/dt^2$ and taking the time derivative of any sinusoidal displacement twice), and eliminating p and z by combining Eqs. (2) and (3), we find the relationship between k and ω:

$$\rho\omega^2/k = S/2 \tag{4}$$

$$k = 2\rho\omega^2/S \tag{5}$$

From this we can find the wave speed

$$c = \omega/k = S/(2\rho\omega) \tag{6}$$

c has units of m/s as it must (to check, recall that $S = Pa/m = kg/(m^2s^2)$, $\rho = kg/m^3$, $\omega = 1/s$). c is proportional to S/ρ, stiffness over mass, as expected. It is proportional to $1/\omega$, showing that at every location in the cochlea the wave speed varies with frequency, decreasing as frequency increases: the cochlear traveling wave is a "dispersive" wave.

In addition to stiffness, the mechanical impedance of the BM will also have resistance, which we will also normalize to area, $r(kg/(sm^2)$. The force due to stiffness is proportional to displacement, and the force due to resistance is proportional to velocity; when the pressure across the OCC works against resistance as well as stiffness, Eq. (3) becomes

$$2p = -(Sz + rv_z) \tag{7}$$

where v_z is the z component of velocity. $v_z = dz/dt = i\omega z$, where the imaginary i is the mathematical representation of the fact that for sinusoidal motions, velocity and displacement are 90 degrees out of phase. To see this, picture a swing in motion: velocity is a maximum when displacement is passing through its zero position.

With the resistance term added to the stiffness term, Eq. (5) becomes:

$$k = 2\rho\omega^2/(S + i\omega r) \tag{8}$$

Using the property of imaginary numbers that $i^2 = -1$, rewrite Eq. (8) as

$$k = (2\rho\omega^2)(S - i\omega r)/(S^2 + (\omega r)^2) \sim (2\rho\omega^2)(S - i\omega r)/S^2 = 2\rho\omega^2/S - i2\rho r\omega^3/S^2 \tag{9}$$

where the approximation holds as long as $S >> \omega r$ (say, at least twice as large). This approximation means the mechanical impedance of the BM is stiffness dominated. The approximation is reasonable (Dong and Olson, 2009) and it keeps the algebra simpler. The real part of k,

$$k_r(x) = 2\rho\omega^2/S(x) \tag{10}$$

is what we described above as "the wavenumber" k, setting the wavelength and wave speed. As a reminder that S, r and thus k are functions of x, they are written $S(x)$, $r(x)$ and $k(x)$ in Eqs. (10) and (11). The imaginary part of k,

$$k_i(x) = -2\rho r(x)\omega^3/S(x)^2 \tag{11}$$

forms an exponential term like $e^{k_i x}$ (but not exactly, as will be explained just below), and this decreasing exponential is what brings down the amplitude of the pressure wave.

There is one final twist before we can plot the pressure wave that started in Eq. (1): Because k_r and k_i are functions of x, we can't simply multiply k_r times x to get $k_r x$, we have to take the integral $\int_0^x k_r(x')dx'$. Similarly, we have to take the integral $\int_0^x k_i(x')dx'$. Finally, the pressure wave, Eq. (1), can be written (with A equal to amplitude of the pressure at $x = 0$):

$$p(x) = Ae^{\int_0^x k_i(x')dx'} cos\left(\int_0^x k_r(x')dx' - \omega t\right) \tag{12}$$

To find the displacement of the BM, $z(x)$, we go back to $2p = -(Sz + rv_z) = -zS - i\omega zr$. Thus $z = -2p/(S + i\omega r)$. For simplicity we'll use the approximation from above, that the BM's mechanical impedance is dominated by stiffness ($S >> \omega r$), which allows us to write $z = -2p/S$. However, we'll retain the resistance to figure the phase of the displacement relative to pressure, which is $\phi_z = arctan(-\omega r/S)$. ϕ_z is close to zero when $S >> \omega r$.

We proceed to plot p and z, as amplitude and phase, and the resulting waveforms. To do the integrals computationally, one decides on dx, something like 1/1000 of the length of the uncoiled cochlea. We use the matlab function cumsum (cumulative sum) multiplied by dx to do the integrals. For the functional forms of $S(x)$ and $r(x)$, we'll use the values in Siebert's 2D, short-wave paper (Siebert, 1974). Siebert assumed a stiffness that decreased exponentially with distance from the base. Decreasing stiffness causes the wave to slow down and the displacement to increase in amplitude. In the absence of a stiffness variation, there would still be a wave but it would not slow as it traveled from base to apex. In Siebert's model, resistance is an exponential function that increases with distance from the base. The resistance causes the wave to eventually decrease in size, producing the displacement peak. The results from Siebert's model for a 2 kHz stimulus, subject to the simplifying approximation noted above, are in Fig. 8. In this discussion standard MKS units (kg, m, N) were used. However, Siebert used cgs units (g, cm, dynes etc) and those units are used in the model program of Fig. 8. In the displacement plot cms were converted to nanometers to emphasize the nano-scale of the motions. The model output shows a snapshot of the spatial wave.

The 2D model is not a realistic representation of the cochlea and it cannot be used to make quantitative predictions, but it does illustrate some of the important features of cochlear mechanics. The ability to "play around" with a simple cochlear model can be very useful for developing understanding. It is easy to input different variations, for example negative resistance over a limited longitudinal extent (as will be explored later), a localized increase in stiffness that might occur with a cochlear implant, the effect of including BM mass (for this subtract $m\omega^2$ from S, with m normalized to area so having units of kg/m^2 or g/cm^2). More realistic and detailed versions of the passive traveling wave model are in (de Boer, 1980, 1984; Lighthill, 1981; Taber and Steele, 1981; Steele and Taber, 1979a).

Tectorial Membrane

The fundamental role of the TM is to be the thing the stereocilia push against and thus activate MET channels, which will be described in Section "MET Channel Mechanics and the Basis for Nonlinearity". The coupling is direct in the case of OHCs, whose

```
% m file Siebert_easy

delx=.01; % cm step size
x=[0:delx:3.5]; % x is variable along cochlea,
                % which is 3.5 cm long
rho = 1; % g/cm^3  density of cochlear fluid

% r and s are resistance and stiffness
% per unit area of the basilar membrane
s = 2e8*exp(-1.5*x); % dynes/cm^3
r = 5*exp(2.25*x); % dynes sec/cm^3

% f = stimulus frequency
f = input('what is the frequency in Hz (2000)?');
w = 2*pi*f;  % radian frequency 2*pi*f

% Analysis below has been simplified by
% assuming s is bigger than wr (at least 2 times as big)
%%%%%%  %real and imaginary parts of wavenumber k
ki=-2*rho*w^3.*r./(s.^2);
kr=2*rho*w^2./s;
%%%%%% computational integral from 0 to point x
krx=delx*cumsum(kr);
kix=delx*cumsum(ki);

%  pressure at the basilar membrane.
A = 2;  % input pressure amplitude units dynes/cm^2
p_amp = A*exp(kix);
p_phase=-krx;

subplot(3,2,1); plot(x,p_amp,'k','linewidth',1.5);
title('Pressure at BM');
xlabel('cm'); ylabel('pressure amp, dynes/cm^2');
xlim([0 3.5])

subplot(3,2,3); plot(x,p_phase/(2*pi),'k','linewidth',1.5);
axis([0 3.5 -6 1]);
xlabel('cm'); ylabel('pressure phase, cycles');
%The waveform of the pressure at the BM:
pwave=p_amp.*cos(p_phase);

subplot(3,2,5);
plot(x,pwave,'k','linewidth',1.5);
xlim([0 3.5])
xlabel('cm'); ylabel('pressure wave, dynes/cm^2');

% ******displacement of BM in nm  ***************
BM_amp=2*p_amp./s;
BM_phase=p_phase+atan2(-w.*r,s); % in radians here

subplot(3,2,2); plot(x,10^7*BM_amp,'k','linewidth',1.5);
title('BM displacement');
xlim([0 3.5])
xlabel('cm');ylabel('BM amp, nm');

subplot(3,2,4); plot(x,BM_phase/(2*pi),'k','linewidth',1.5);
axis([0 3.5 -6 1]);
xlabel('cm');ylabel('BM phase, cycles');
%waveform of the BM displacement:
vwave=10^7*BM_amp.*cos(BM_phase);

subplot(3,2,6);
xlim([0 3.5])
plot(x,vwave,'k','linewidth',1.5);
xlim([0 3.5])
xlabel('cm'); ylabel('displacement wave, nm');
```

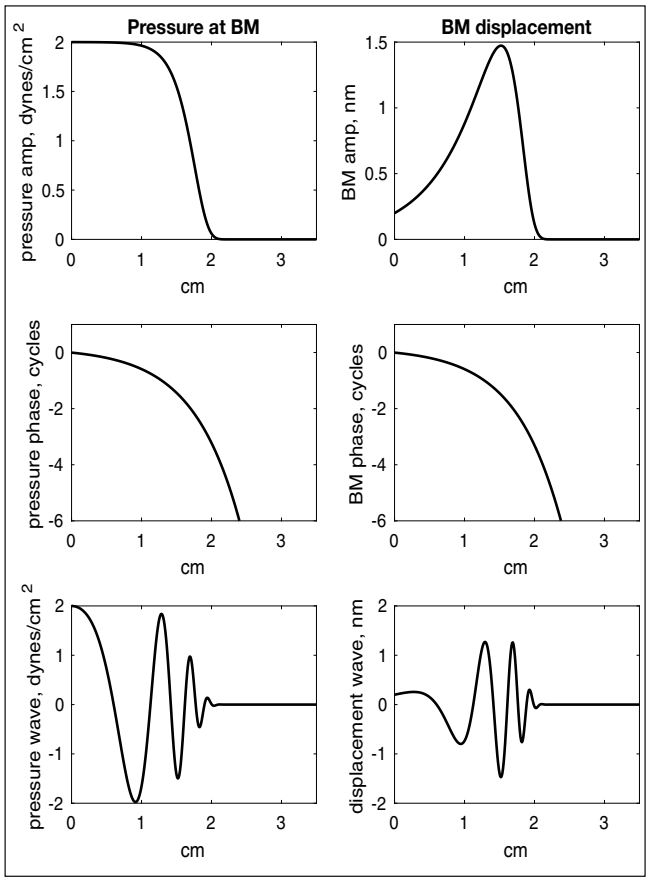

Figure 8 On the left is the matlab code describing the 2D shortwave model. On the right are the results from the code when the input frequency is 2 kHz.

stereocilia tips are embedded in the TM surface, and via fluid forces for the IHCs, whose stereocilia reach up to nearly touch the TM's underlying surface (Lim, 1980). By weight the TM is $\sim$ 97% water, and $\sim$ 50% of its dry weight is protein, with collagen up to 50% of the protein content, and three glycoproteins, α-tectorin (Tecta), β-tectorin (Tectb) and otogelin making up $\sim$ 50% (Weiss and Freeman, 1997; Richardson et al., 2008). These glycoproteins contain fixed charge, which brings water into the TM, endowing it with its gel-properties. They are almost unique to the inner ear and have been experimentally mutated in highly informative studies of TM function (Gummer et al., 2017; Richardson et al., 2008). Like the BM, the collagen fibers of the TM are primarily radial, and this makes it stiffer in the radial than in the longitudinal direction (Gavara and Chadwick, 2009). Its gelatinous water-rich structure appears to keeps it floating gently atop the hair cells, with its radial fibers providing stiffness so that the stereocilia pivot when driven

by sound-induced motions between the RL and TM (Gueta et al., 2008). The TM's mechanical properties were studied in-situ by point stiffness measurements in gerbil (Richter et al., 2007) and a longitudinally varying stiffness, smaller in the apex than the base, was observed. Its mechanical properties have also been studied when excised, in both dynamic and static measurements (Gavara and Chadwick, 2009, 2010; Freeman et al., 2003a, 2003b). These studies affirmed the anisotropic properties, longitudinal variations and sensitivity to osmotic forces. The Young's modulus of the bulk TM material is orders of magnitude less than that of the BM (Liu et al., 2015b). The TM's shape is different from the BM and its mode of motion is different; while the BM is anchored on two sides and bends like a set of radial beams, the TM is firmly anchored at the limbus on the medial side and relatively loosely at its lateral edge (**Figs. 2** and **3**) (Lim, 1980; Richardson et al., 2008), and is likely to pivot and elongate/compress radially when sound stimulation enters the cochlea. When the Tecta glycoprotein was genetically knocked out of the tectorial membrane, the TM lifted off from the OC, and in in-vivo experiments tuning at the BM was greatly reduced (Legan et al., 2000). Intriguingly, knocking out the Tectb protein could *enhance* tuning at the BM in in-vivo experiments, perhaps due to reduced longitudinal coupling (Russell et al., 2007). The properties of the tectorial membrane and the Tectb mutant were recently explored in a combined experimental/FEM study (Lemons et al., 2019). That paper is a rich source of quantitative information on TM properties, both new findings on the spatial extent of TM motion, and discussion and comparisons with previous findings. One of the messages of the paper is that the TM's radial stiffness enhances the simultaneity of stimulation of each radial group of OHCs (Gavara and Chadwick, 2009). This underscores the primary function of the TM: to properly stimulate hair cells. In this vein, the TM was recently shown to contain a relatively high concentration of Ca^{+2}, particularly in the region of stereocilia attachment. Ca^{+2} is important for maintaining MET channel operating point, thus in addition to its mechanical role in hair cell excitation, the TM affects hearing sensitivity by maintaining the ionic environment of the MET channel (Strimbu et al., 2019).

When excised and driven in the radial direction at auditory frequencies, the TM exhibits radial motion whose pattern moves longitudinally as a traveling wave, interpreted as a mechanical shear wave (Ghaffari et al., 2007). The TM waves had similar wavelengths as in vivo BM traveling waves, which are less than 1 mm near a stimulating frequency's best place (Ren, 2002). The TM waves provided an indirect measurement of TM stiffness (recall the relationships between wave speed and mechanical properties like stiffness in Section "**Passive Cochlear Models: Physics of the Cochlear Traveling Wave**") and supported the idea that the cochlea operated as a coupled traveling wave system. The TM has been implicated in tuning cochlear amplification in cochlear models. More on this in Section "**Layer 3: Current Thinking and Explorations on How the Cochlear Amplifier Works,**" on modern cochlear models.

Back to the Traveling Wave

This section closes with a discussion of several notable studies relating to the cochlear traveling wave. (1) Glides and the traveling wave. Section "**Passive Cochlear Models: Physics of the Cochlear Traveling Wave**" noted that at a given location the wave speed was inversely proportional to frequency (**Eq. 6**). A stimulus like a click contains many frequencies, which are dispersed in the cochlear traveling wave. With a click stimulus, at any one location in the cochlea, low frequencies arrive before higher frequencies, resulting in an upward "glide" of instantaneous frequency in the auditory nerve response (Carney et al., 1999). Glides have also been noted in BM motion responses (Recio et al., 1998; De Boer and Nuttall, 1997). It is interesting and informative that in the apical, low frequency region of the cochlea, frequencies both below and above the BF can arrive before BF frequencies. Thus, while traveling to that location, tones both higher and lower than the BF travel faster than the BF tones. This prediction does not come out of a simple traveling wave model (Shera, 2001a; Temchin et al., 2011). (2) The cochlear traveling wave is a passive property of the tissue that does not require cells. The traveling wave remains post-mortem; after hours post-mortem the peak shifted down in frequency (Cooper et al., 1999). The traveling wave was present in cochleae in which the OC had been ototoxically removed from the BM with intratympanic neomycin; the response peak was at a lower frequency than in untreated cochleae (Eze and Olson, 2011). These findings indicate that the stiffness that governs the traveling wave is reduced when the cells are damaged or missing, which is expected in light of stiffness measurements at the BM in which cells added significantly to point stiffness (Olson and Mountain, 1994; Naidu and Mountain, 1998). (3) The stiffness of the OCC and its longitudinal variation is a key physical property. Stiffness is based on cell and tissue components, dimensions, and geometrical arrangement. Tabulations of these quantities are in recent cochlear modeling papers (Liu et al., 2015b; Zhou and Nam, 2019; Motallebzadeh et al., 2018; Meaud and Grosh, 2012). Because different information is available for different mammals, these tables often derive from a variety of mammals, typically gerbil, guinea pig, rat and mouse. Several papers emphasize how functional stiffness is determined from mechanical properties and geometry, and relate these properties to the tonotopic map (Liu et al., 2015b; Kapuria1 et al., 2017; Fleischer et al., 2010); see also (Olson et al., 2012). (4) Other traveling wave components: The pressure component of the traveling wave was measured much later than the motion component (Olson, 2001; Kale and Olson, 2015). When measured close to the BM it was found to be tuned and nonlinearly enhanced, similar to BM motion. These observations supported the concept of "cochlear amplification" that will be described in more detail below: that sharp cochlear tuning and enhancement of BM motion is due to an internal energy source within the OCC. Evidence for the traveling wave in cochlear microphonic measurements (CM) date back to the 1970s (Dallos and Cheatham, 1971; Dallos et al., 1974). The CM is an extracellular voltage, generated by the electrical response of hair cells to the motion of the sensory tissue. When measured locally within the cochlea as local CM (LCM), its tuning, nonlinearity and traveling wave phase excursion are similar to that of BM displacement (Fridberger et al., 2004; Dong and Olson, 2013a; Fallah et al., 2019). (When measured at the round window, the CM is a gross cochlear response with contributions from many hair cells, and is used as a diagnostic of cochlear condition.) Examples of pressure and LCM responses measured at the BM are in **Fig. 9**C–F. This figure brings us to layer 2, on the cochlear amplifier.

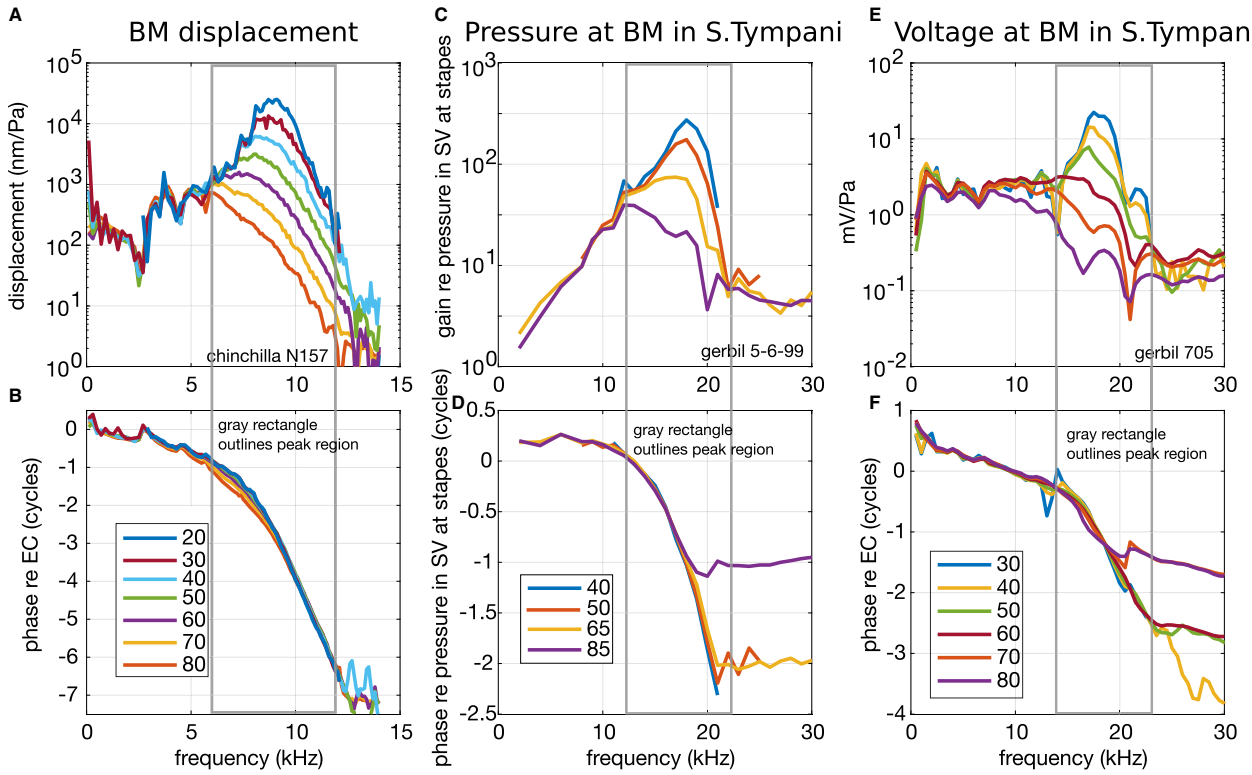

Figure 9 Three examples of pure-tone frequency responses, from three different preparations and redrawn from the originally published plots. (A and B) BM displacement data from the 9 kHz region of chinchilla, and referenced to ear canal pressure (Rhode, 2007a). (C and D) Pressure data measured close to the BM at the 18 kHz region of gerbil and referenced to the scala vestibuli pressure in the cochlea at the stapes (Olson, 2001). (E and F) Voltage data measured close to the BM (local cochlear microphonic) at the 18 kHz region in gerbil and referenced to ear canal pressure (Wang et al., 2019). Gray rectangles outline the region of amplification.

Layer 2: Cochlear Nonlinearity and the Cochlear Amplifier

The discovery of enhanced, nonlinear tuning at the BM established the preeminence of the cochlear amplifier for cochlear processing. Fig. 9 shows three examples of frequency responses, from three different preparations. These are all responses garnered with pure tone stimulation. The responses are shown normalized to a standard input, in order to make the nonlinearity stand out. On the left are BM displacement data from the 9 kHz region of chinchilla, referenced to ear canal pressure. In the middle are pressure data measured close to the BM at the 20 kHz region of gerbil, referenced to the scala vestibuli pressure at the stapes. On the right are voltage data measured close to the BM in gerbil, referenced to ear canal pressure. They all show several key features: (1) Phase accumulating through several cycles, evincing the traveling wave as described in Fig. 4. (2) Striking nonlinearity in the BF peak region. (3) Lack of nonlinearity in the sub-BF region except at high SPL in the LCM measurement. The BF-region peak-enhancing nonlinearity is the primary experimental observation of the cochlear amplifier. (4) A plateau in amplitude and phase starting at a frequency above the BF peak, termed the "fast mode" response: The in-out motion of the stapes, in addition to launching a pressure/motion traveling wave, produces a nearly space-filling compression-rarefaction pressure, termed the fast mode because it is timed with the stapes motion with almost no delay (Fig. 9C and D above 20 kHz). Following the traveling wave's post-peak decline, the fast mode remains and produces a residual motion, which can excite hair cells (Fig. 9A and B above 13 kHz). The fast mode was predicted and has been explored (Olson, 2013; Peterson and Bogert, 1950). In the next sections the basis for cochlear nonlinearity and amplification will be described.

MET Channel Mechanics and the Basis for Nonlinearity

In the cochlea everything depends on the hair cell stereocilia bundle. The stereocilia are actin-packed rods that emerge from the tops of the hair cells. Mechanoelectric transduction occurs when the bundle pivots, due to shearing motion between the reticular lamina and the tectorial membrane (Fig. 2B), opening cation-selective channels in the tips of the stereocilia. A cartoon of the hair bundle tips (TM not included) is in Fig. 10 and a beautiful image of the stereocilia bundles of mouse OHCs is in Fig. 11.

The mechanics of the hair bundle and the identity and properties of the transducer channel have been the focus of scores of studies and review articles. A description of the stereocilia bundle and its spatial variation along the cochlea is in (Lim, 1986);

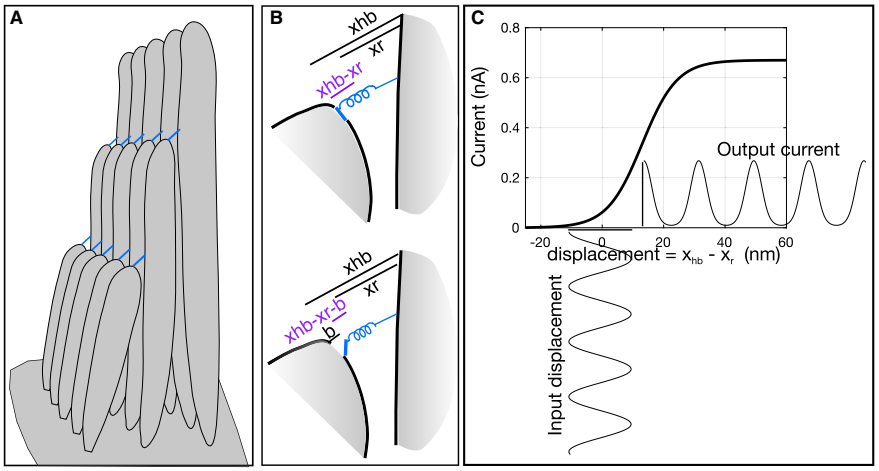

Figure 10 A) stereocilia bundle with tip links in blue springs. (B) Zoom in of tip link, showing closed (top) and open states (bottom). For this position of the hair bundle (x_{hb}) the spring is stretched a distance $x_{hb} - x_r$ when closed and $x_{hb} - x_r - b$ when open. b is the size of the gate swing. x_r is the unstretched/uncompressed state of the spring (which is not necessarily the operating point of the hair bundle). (C) Boltzmann function description of transducer current, based on data from **Fig. 4**E in (Fettiplace and Kim, 2014). The Bolzmann parameters used in the fit were $kT/F_G = 5.7$ nm and $x_r = 13$ nm. The measurements were made on an outer hair cell in a P7 mouse, recorded with 1 mM EGTA intracellular buffer, at 23 degrees C. Panel (C) shows the predicted distortion in the output current that would occur with a 10 nm peak sinusoidal displacement of the hair bundle tip.

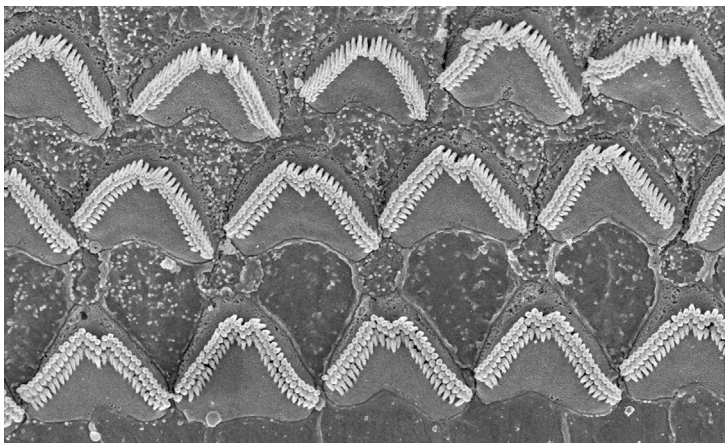

Figure 11 Top-down view of mouse OHCs, showing the characteristic V or W-shaped hair bundles. Inner hair cells are not included in the micrograph, and would be below. Courtesy of M'hamed Grati and Bechara Kachar (NIH/NIDCD).

a comprehensive review of mechanotransduction is in (Fettiplace and Kim, 2014), of identifying the transduction channel is in (Effertz et al., 2015) and of stereocilia physiology is in (Velez-Ortega and Frolenkov, 2019). Among the key findings are the location of the channel (Lumpkin and Hudspeth, 1995; Hudspeth, 1982; Beurg et al., 2009), the probable identity of the channel (Effertz et al., 2015; Pan et al., 2013), the presence of adaptation in vestibular hair cells (Eatock et al., 1987), the mechanics of channel opening (Howard and Hudspeth, 1988), fast adaptation in mammalian cochlear hair cells (Ricci et al., 2000), and most recently the nanomechanics of the channel and tip-link proteins (Sotomayor et al., 2012; Bartscha et al., 2019; Corey et al., 2017; Oroz et al., 2019).

The stereocilia bundle in mammals is composed of three (sometimes four) rows of stereocilia, with approximately 100 per bundle. An individual stereocilia is ~500 nm wide at the top, tapering to ~200 nm at the bottom. The stereocilia are arranged in a staircase pattern of increasing height. Deflecting toward the tallest/shortest row opens/closes the channels. The stereocilia are connected by a variety of linkages (Hackney and Furness, 2013; Karavitaki and Corey, 2010), the most famous being the tip link, located near the top of the stereocilia, that connects the stereocilia in one row to the next row (Pickles et al., 1984). The tip link itself is ~150–185 nm long, formed by two or three twisted protein strands composed of cadherin-23 and protocadherin-15 (Kachar et al., 2000; Kazmierczak et al., 2007). The channel is located at the bottom of the tip link with two channels per tip link (Beurg et al., 2009). Thus, an individual hair cell has ~120 channels. The individual channel is either open or closed (two states) and the graded receptor current response of a hair cell results from the probablility that an individual channel is open,

summed over the channels in the hair cell. The open probablility is altered by the mechanical stimulus to the bundle, in particular, when it is pulled to be more probably open or pushed to be less probably open by the shearing motion between the tectorial membrane and reticular lamina. The probability that the channel is open is given by a two-state Boltzmann distribution, as in **Fig. 11**C, redrawn from a fit to experimental data from a mouse OHC, **Fig. 4**E of (Fettiplace and Kim, 2014). From **Fig. 11**, when the channels were fully open ($P_o = 1$), the transducer current through the OHC was ~0.67 nA.

The MET channel is most likely the component of the cochlea that produces the observed nonlinearity in cochlear responses. Therefore, the mathematical function that describes its opening deserves a few lines of explanation, emphasizing the basic physics and the key parameters. Additional details can be found in (Fettiplace and Kim, 2014).

Boltzmann's probability function states that the probability of a system being in a particular state is proportional to $e^{-\varepsilon/kT}$, where ε is the energy associated with that state, k is Boltzmann's constant and T is temperature in Kelvin units (K). (For reference, mammalian body temperature is ~310 K and Boltzmann's constant is 1.38×10^{-23}Joules/K.) Thus, the probabilities of being open and closed are

$$P_o = Ae^{-\varepsilon_o/kT} \tag{13}$$

$$P_c = Ae^{-\varepsilon_c/kT} \tag{14}$$

$P_o + P_c = 1$ so we can solve for A: $A = 1/[e^{-\varepsilon_o/kT} + e^{-\varepsilon_c/kT}]$, and

$$P_o = e^{-\varepsilon_o/kT} / \left(e^{-\varepsilon_o/kT} + e^{-\varepsilon_c/kT}\right) \tag{15}$$

which can be rearranged as,

$$P_o = 1/\left(1 + e^{(\varepsilon_o - \varepsilon_c)/kT}\right) \tag{16}$$

The energy involved in opening and closing the channel is due to stretching the gating spring, with spring constant S_G. **Fig. 11** shows that the spring is stretched an amount $x_{hb} - x_r$ when the channel is closed and $x_{hb} - x_r - b$ when the channel is open. b is the size of the gate swing. Energy in a spring of spring constant S and stretch x is $(1/2)Sx^2$. Thus the energy in the closed and open states is $\varepsilon_c = (1/2)S_G(x_{hb} - x_r)^2$ and $\varepsilon_o = (1/2)S_G(x_{hb} - x_r - b)^2$, respectively. From **Eq. (16)**, the important thing is the difference, $\varepsilon_o - \varepsilon_c$. Taking the difference of the two energies results in cancellation of the $(x_{hb} - x_r)^2$term, and we are left with:

$$\varepsilon_o - \varepsilon_c = (1/2)S_G\left(b^2 - 2b(x_{hb} - x_r)\right) \sim -S_G b(x_{hb} - x_r) \tag{17}$$

where the approximation results because b is small compared to $(x_{hb} - x_r)$ and thus b^2 can be neglected. With this, **Eq. (16)** becomes

$$P_o = 1/\left(1 + e^{-S_G b(x_{hb} - x_r)/kT}\right) = 1/\left(1 + e^{-F_G(x_{hb} - x_r)/kT}\right) \tag{18}$$

a two-state Boltzmann probability distribution, as shown in **Fig. 11**C. The product of the spring constant and the gating swing, $S_G b$, is equal to the gating force, F_G, a quantity that has been measured, with values of ~0.5 pN (Fettiplace and Kim, 2014). The slope of the probability function, dP_o/dx_{hb}, is maximum when $x_{hb} = x_r$, and at that point is equal to $(1/4)F_G/kT$. The channel is most sensitive to hair bundle deflection when operating around this point, with the gating spring neither compressed nor stretched. In vivo, the operating point of hair cell stereocilia appears to be reasonably but not perfectly centered at x_r. A centered operating point seems optimal for the OHCs' function in amplification (Section "**OHC Electromechanics and the Basis of Cochlear Amplification**"). For the IHCs, whose major role following mechanoelectric transduction is transmitter release, it is better for the operating point to be somewhat uncentered in order to generate a DC component of transducer current (Dallos, 1986; Cody and Russell, 1987).

In addition to operating point, an important aspect of the Boltzmann distribution is operating range – the range of stereocilia deflection that takes the channels from the all-open to the all-closed state. From **Fig. 11**C, this is only ~ 40 nm. Thus, the operating point of the stereocilia must be maintained almost to the nanometer in order that the MET channel does not go out of its operating range. The operating point of the MET channel is likely disturbed in some forms of Meniere's Disease and sudden hearing loss. Operating point changes have been studied with both mechanical manipulations such as low-frequency acoustic biasing or injection of fluid, and indirect manipulations such as osmotic changes or injection of furosemide (Wang et al., 2019; Sirjani et al., 2003; Salt et al., 2009; Kirk et al., 1997).

By considering **Fig. 11**B, when the stereocilia pivot to the right, and MET channels swing open, the spring stretch is reduced, and the spring's restoring force will be reduced. This corresponds to a negative stiffness: pulling on the bundle to move a given distance x, when channels open, the force required (which had been increasing) suddenly is reduced. When the bundle pivots left the opposite occurs – the spring force abruptly increases when the channels close. Thus, with acoustic stimulation, as the hair bundle moves back and forth through the operating range of the channels, the bundle stiffness goes through a minimum at the location where half the channels are open (Howard and Hudspeth, 1988). Negative stiffness can give rise to active, spontaneous bundle motion, which might be involved in cochlear amplification, and activity in other hair cell systems (Martin et al., 2003; OMaoileidigh and Julicher, 2010; Kennedy et al., 2005).

OHC Electromechanics and the Basis of Cochlear Amplification

The amazing ability of OHCs to move and exert forces in step with transmembrane voltage, a property known as "electromotility", is at the heart of mammalian cochlear amplification. OHC electromotility was discovered in 1985 (Brownell et al., 1985). It is based in the protein Prestin, which studs the OHC lateral membrane (Zheng et al., 2000). **Fig. 12**A shows an electromotility experiment in which the OHC was held by the electrode that was providing the voltage clamp, and the voltage-dependent displacement of the cuticular plate at the apex was measured (Ashmore, 1987). OHC electromotility has been described as an area motor, in which a conformational change of the Prestin protein causes the cell to vary between elongated and shortened states (Iwasa, 2001). **Fig. 12**B shows an example of an OHC strain (percent length change) with change in voltage. The OHC was stimulated through a 250 mV range to trace out the entire range of length change (Adachi et al., 2000). The OHC length varied between two extreme states, in which the OHC was either fully contracted or fully elongated, and was adequately fit by a 2-state Boltzmann function in **Fig. 12**B. The 2-state Boltzmann was introduced above in **Eq. (16)**, and here the energy difference term from **Eq. (17)** is equal to $q_l(V - V_{mp})$, where $V_{mp}$is the horizontal midpoint of the function, and q_l, the unit charge of the motor, was found to be $\sim 0.8e$ (Adachi et al., 2000) (e is the elemental charge of an electron.) 20 mV peak-to-peak is the maximum excursion one would expect for the OHC receptor voltage based on both in vivo and in vitro measurements (Cody and Russell, 1987; Johnson et al., 2011). The operating voltage range of OHC somatic motility observed in **Fig.12**, ~100 mV, is substantially larger than this maximum 20 mV peak-to-peak receptor voltage. Thus, the output response scales nearly linearly with input: the response variation over 20 mV is nearly a straight line, regardless of the operating point. The 20 mV scale bars in **Fig. 12**B illustrate this. This is different than the situation with the MET channel (**Fig. 11**), where the input range of displacement was similar in size to the operating range of the MET channel. Thus, OHC electromotility is thought to be the basis for amplification, but not for nonlinearity, which is most likely the MET channel (Santos-Sacchi, 1993; Geisler et al., 1990).

The operation of OHC electromotility to frequencies exceeding 10 kHz has been observed in vitro (Frank et al., 1999; Santos-Sacchi and Tan, 2018), and detected in vivo in experiments in which intracochlear voltage applied at frequencies up to 100 kHz continued to elicit BM motion responses (Grosh et al., 2004). OHC electromotility has been used to probe micromechanics in in-vitro preparations, because applied current can be used as a mechanical stimulus via electromotility (Karavitaki and Mountain, 2007; Nowotny and Gummer, 2011). **Fig. 12** emphasizes electromotility, but more important quantities to consider are the electrically-induced forcing and power transferring capabilities of OHCs (Rabbitt et al., 2019). The isometric force exerted by a voltage-driven OHC is ~.01–0.1 nN/mV (Frank et al., 1999; Iwasa and Adachi, 1997). In (Frank et al., 1999) this was frequency independent through 20–50 kHz, the highest frequency that could be measured reliably. Measured electromotility and predicted power transfer vary with OHC size (Frank et al., 1999; Rabbitt et al., 2019). Along the length of the cochlea, OHC length varies by a factor greater than three in guinea pig (shorter/longer in the base/apex), and by almost a factor of eight when comparing across species from bat to mole rat (Pujol et al., 1991). Recent measurements have emphasized the importance of maintaining the OHC in relatively natural conditions of ionic concentration, holding potential, and mechanical load to understand its operation in vivo (Johnson et al., 2011; Santos-Sacchi and Tan, 2018; Rabbitt et al., 2019; Santos-Sacchi et al., 2006, 2017; Iwasa, 2018). Much remains to be understood about the Prestin molecule, OHC electromotility and how it functions within the cochlear amplifier.

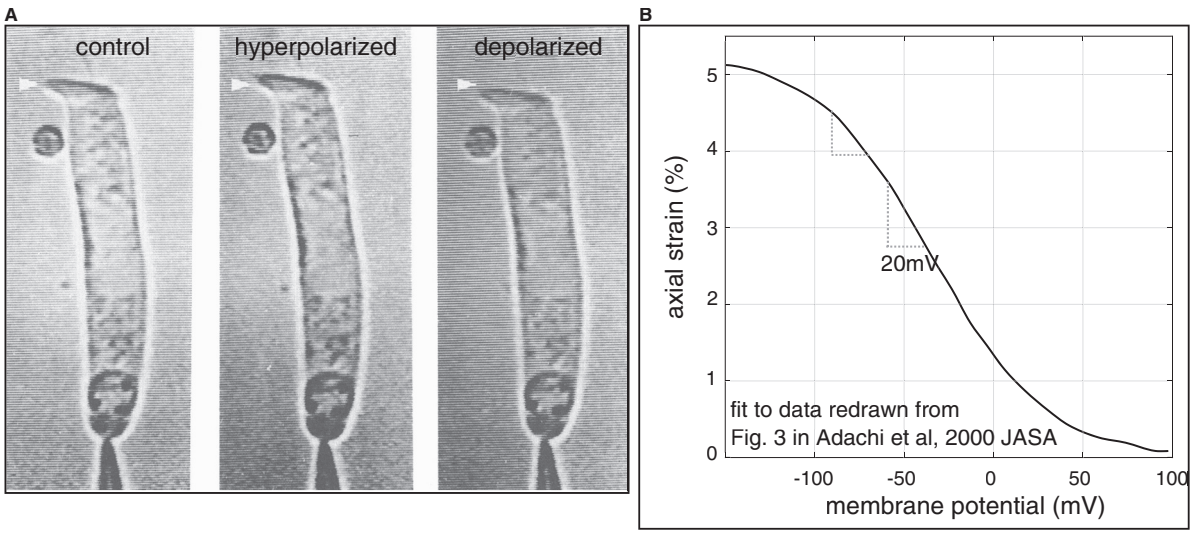

Figure 12 A) Images from Ashmore (Ashmore, 1987). OHC under voltage clamp (electrode at bottom) elongating and contracting when hyperpolarized and depolarized. (B) From Adachi et al. (Adachi et al., 2000). Axial strain (length change/length) varies from fully engaged to fully compressed over ~250 mV. The response can be fit with a 2-state Boltzmann shown here. The 20 mV scale bar indicates the maximum expected OHC receptor potential and over that range the strain would scale nearly linearly with voltage. For an OHC of length 55 μm, the total length change is ~3 μm.

Active stereocilia mechanics might provide additional force for amplification, but most studies agree that OHC somatic forces are the primary amplification mechanism, at least in the basal and mid-region of the cochlea where amplification is most fully characterized (Johnson et al., 2011; Meaud and Grosh, 2011; Mellado Lagarde et al., 2008; Shuping and He, 2005). Nevertheless, because they control the current through the OHC and thus the OHC voltage, hair bundle and MET channel mechanics have a fundamental role in cochlear amplification. As an efficient but perhaps overly simplified analogy, OHC electromotility is the engine of amplification, and the OHC bundle (and its connection to the TM) is the foot on the gas pedal (Zhou and Nam, 2019; Meaud and Grosh, 2011). Some possible forms of the control mechanism will be discussed in Section "**Layer 3: Current Thinking and Explorations on How the Cochlear Amplifier Works**."

The effect of MET current nonlinearly driving OHC forces was illustrated in the pronounced nonlinearity in the BF peak region (**Fig. 9**). These were studies using pure single tones as stimulus. Nonlinearity also gives rise to interactions between two simultaneously delivered tones, often studied as two-tone suppression (Fahey et al., 2000). Two-tone suppression was first observed in auditory nerve experiments, in which the introduction of a second tone could have a profound effect on a fiber's firing pattern, even eliminating firing entirely (Fahey and Allen, 1985). Often in two-tone suppression experiments, one tone is held at the frequency of the local BF and the ability of a second tone to suppress that response is determined. These experiments revealed that tones slightly above the BF, which would peak slightly basal, were the strongest suppressors (Delgutte, 1990; Sachs and Kiang, 1968). This finding, indicating that a region basal to the peak is involved in amplification at the peak, was also observed in BM motion studies (Robles and Ruggero, 2001; Versteegh and vanderHeijden, 2013), and recently in an OCT-based study of OCC motion (Dewey et al., 2019). Many, but not all of the neural two-tone responses can be understood in terms of mechanical responses measured at the BM (Geisler et al., 1990; Rhode, 2007b; Geisler and Nuttall, 1997).

Modern Measurements of OCC Motion

Optical coherence tomography (OCT) based motion measurement was introduced to cochlear mechanics by the research groups of Freeman (Hong and Freeman, 2006) and Nuttall (Wang and Nuttall, 2010). Although it is a project to implement, OCT is becoming fairly widely used in the cochlear mechanics community for measurements of OCC motion. The research group of Oghalai has done extensive work in the apical region of the mouse cochlea, which can be probed with their purpose-built instruments without opening the bone (Lee et al., 2016; Gao et al., 2013). A set of published data from that lab is in **Fig. 13** (Lee et al., 2016). Panel 1 (from their **Fig. 1**) is a B-scan, a two-dimensional image with the vertical axis corresponding to the direction of the light source - into the preparation. One can appreciate both the amazing ability to see the intracochlear structures, and the fuzziness of the image. In spite of the fuzziness, different components can be discerned: the BM, the TM, the RL and OHC regions. The B-scan image was taken by scanning the OCT light beam laterally. If the mirror is arrested, one measures a single A-scan (axial scan). With Spectral Domain OCT (SD-OCT), which is used by most groups (an exception is (Chen et al., 2011) in which Time-Domain OCT was used), the light beam travels through the tissue and is reflected back and is analyzed to construct an A-scan. Three A-scans are shown in panel 2 of **Fig. 13**, and their positions in the B-scan indicated in panel 1. The large peaks on the left of the A-scans correspond to the bony shell (top of the image in panel 1), then there is a broad minimum corresponding to the fluid region (black in the B-scan), and then local maxima corresponding to the structures of interest within the OCC. With further analysis (Lin et al., 2017a; Jacques et al., 2013) it is possible to determine the motion at these locations, or any location within the A-scan, truly simultaneously. The ability to measure motion through the bone, and measure motion simultaneously from many locations, is a leap forward for cochlear mechanics. By measuring sequentially from two angles, Lee et al. (Lee et al., 2016) were able to find both transverse motions (left three columns in lower set of **Fig. 13**, from their **Fig. 2**) and radial motions (right three columns). These data illustrate several of the important findings emerging from this new technique. (1) The traveling wave, evinced by the phase accumulation through many cycles, is present and similar (not to say identical) in all layers (row of panels S-X). (2) The BM's transverse motion (left column) shows the familiar BF-region nonlinearity and lack of nonlinearity in the sub-BF region. (3) Within the organ of Corti (second and third columns from the left) the nonlinearity is strong in the BF region but also present in the sub-BF region at high SPL. OCT-based measurements in the gerbil base have made similar observations of sub-BF nonlinearity within the OCC (Fallah et al., 2019; Cooper et al., 2018). An intriguing finding of the study shown in **Fig. 13** was that radial motion of the TM and RL were tuned relative to the motion of the BM. The OCT technique can be used to explore the differential motions that lead to hair cell excitation and other interesting internal motions. Care has to be taken to avoid artifacts, such as those due to vibrations of the fluid column (Cooper et al., 2018) and signal leakage between adjacent points (Lin et al., 2017b).

Layer 3: Current Thinking and Explorations on How the Cochlear Amplifier Works

One of the primary observations made in **Fig. 9** (Section "**Back to the Traveling Wave**"), was the sub-BF linearity extending up to a frequency of $\sim$ 0.7 BF, followed by the nonlinear BF-peak. The new OCT-based measurements, which have observed sub-BF nonlinearity, muddy the previously clear separation into sub-BF and BF regions. However, the sub-BF nonlinearity behaves differently than the BM-motion-amplifying nonlinearity of the BF-region (Fallah et al., 2019; Dewey et al., 2019). The BF-region nonlinearity is emphasized here in discussing the concepts of several cochlear models.

The recognition of a division into sub-BF and BF regions goes back many years, and was the basis for the early TM resonance models of Zwislocki and Allen (Zwislocki, 1986; Allen, 1980). In those days, the BM-nonlinearity had not yet been measured,

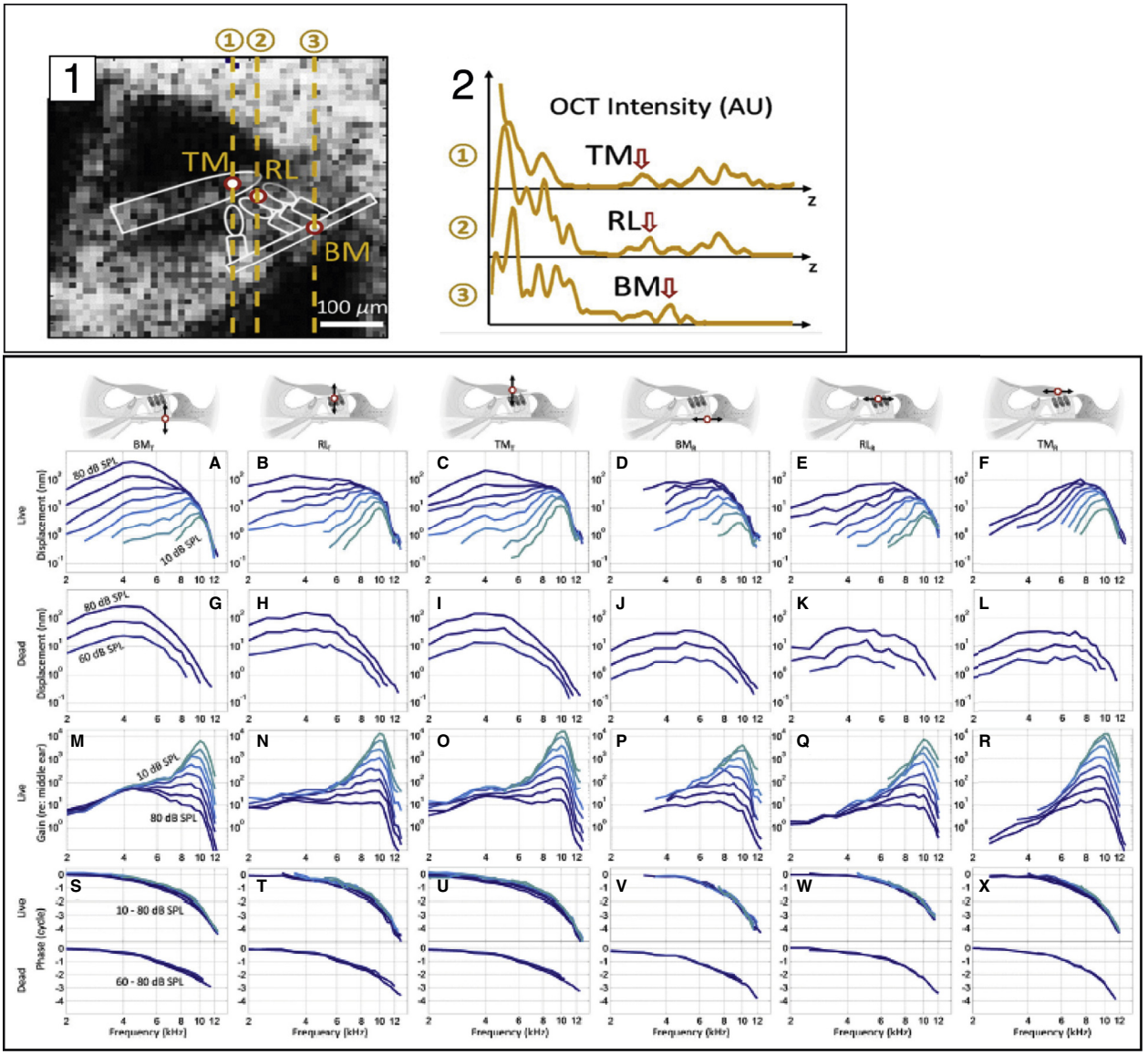

Figure 13 OCT-based displacement measurement in mouse cochlea from **Figs. 1** and **2** of (Lee et al., 2016). Panel 1 shows a B-scan from close to the apex, imaged through the bony otic capsule. The basic structures are resolvable and labeled. The three vertical lines identify the A-scans of Panel 2. By repeatedly taking an A-scan image at high sample rate the displacement of every location in the A-scan can be determined. A-scans were taken from two angles (one of the angles is shown in panels 1 and 2) in order to find motion in radial and transverse directions, as indicated in the sketches in the top row of the lower set of panels. Lower panels show: the magnitude of the displacement in vivo (A–F) and post-mortem (G–L), the normalized magnitude (M–R) and the phase of the displacement in vivo and post-mortem (S–X).

and there was not a concept of amplification, but there were data showing sharp neural tuning in the BF region, and a sub-BF "tail." These two regions were affected differently by cochlear damage (Kiang et al., 1986). After sharp BM motion tuning and nonlinearity were observed, cochlear models were developed to understand it. **Fig. 14** shows three varieties. **Fig. 14**A illustrates the model proposed and developed by Steele's group, based on longitudinal coupling (recall **Fig. 3**E and F) (Yoon et al., 2011). For a stimulus frequency close to a location's BF, wavelength is short, and the tension of the OHC-driven Deiters cells rods is phased properly to inject power into the traveling wave. **Fig. 14**B shows Grosh's group's TM resonance model, which incorporated OHC forces into a model including a TM-resonance, making it active (Ramamoorthy et al., 2007). **Fig. 14**C is one version of a dual-traveling-wave model from Chadwick's group (Lamb and Chadwick, 2011), see also (Cormack et al., 2015). Dual traveling wave models relate to the TM traveling wave discussed in Section "**Tectorial Membrane**", although the concept predates the TM wave observations (Hubbard, 1993; Chadwick et al., 1996). Active traveling wave models have historically been developed as linear, frequency-domain models – for example the models of **Fig. 14**, see also (Neely and Kim, 1986; de Boer and Nuttall, 2000). In these linear active models, the nonlinearity of the active force is approximated by taking different values for different stimulus levels. Nonlinear

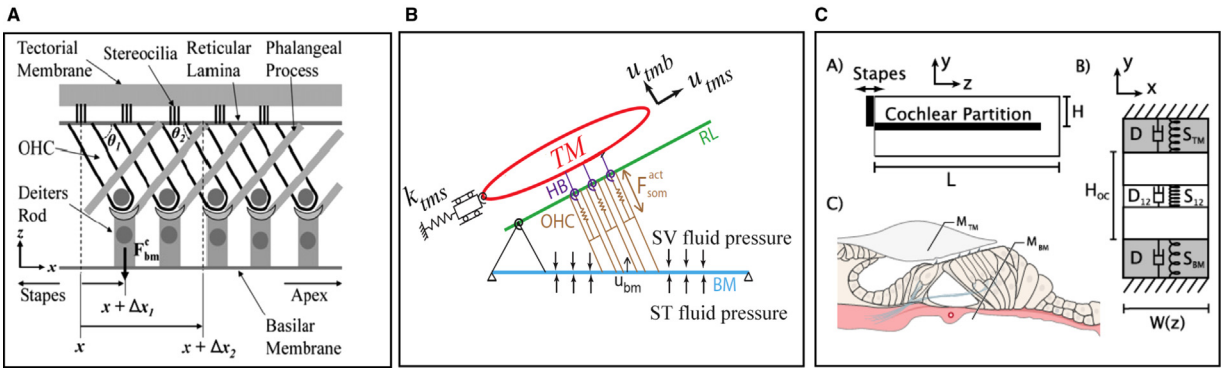

Figure 14 Three conceptualizations of the micromechanics of the organ of Corti. (A) Model emphasizing the importance of longitudinal mechanical coupling (Yoon et al., 2011). (B) Model incorporating a TM mechanical resonance (Ramamoorthy et al., 2007). (C) Model recognizing the layered structure of the OCC would lead to coupled traveling waves (Lamb and Chadwick, 2011). Further discussion is in text.

time-domain traveling wave models have also been developed, and explore both fundamental questions regarding stability (Duifhuis, 2012) and questions such as the effect of hair bundle adaptation on nonlinear responses (Zhou and Nam, 2019; Meaud and Grosh, 2012).

The effect of activity on cochlear responses can be illustrated using the simple linear model developed in **Figs. 7** and **8**. In **Fig. 15** an internal power source is included as a region of negative resistance just basal to the passive peak. In this simple model the internal power source was included very crudely: simply pasted into the code as r (100:150) = -500. In contrast, each of the relatively realistic models described in **Fig. 14** would naturally position the internal power source at the correct place for a given frequency. For example, in the model of **Fig. 14**A, the internal power source becomes effective when the phase starts to rapidly accumulate, which occurs as the peak is approached. The hypothesis that cochlear amplification should be attributed to an internal power source (modeled as a negative resistance) has much support, for example the presence of otoacoustic emissions (Kemp et al., 2008), of OHC electromotility (Rabbitt et al., 2019) and of nonlinearly enhanced pressure at the BM (Olson, 2001). Additional strong support for the internal power source concept is the observation that the large enhancement of response amplitude with decreasing stimulus level is accompanied by very little change in response phase with decreasing stimulus level (**Fig. 9** and **Fig. 13**) (de Boer and Nuttall, 2000). Consider an alternative scenario: if the internal mechanism for amplitude enhancement were due to a mechanism that reduced stiffness, the amplitude would increase but also the wave speed would decrease (recall Section "**Passive Cochlear Models: Physics of the Cochlear Traveling Wave**"), and thus phase accumulation would vary substantially with stimulus level, which is not observed (Kolston, 2000). Observations of the level-independence of zero-crossings in the response to a click are the time-domain corollary to the level-independent phase of frequency-domain results, and also affirm the internal power source conceptualization of cochlear amplification (Shera, 2001b).

A recent experimental finding gave more information regarding the transition between sub-BF and BF regions (**Fig. 16**) (Dong and Olson, 2013a). In simultaneous measurements of OHC-generated extracellular voltage (the LCM as in **Fig. 9**E and F) and BM displacement, at the frequency where amplification began the phase of the voltage transitioned from being in-phase with displacement to leading slightly (**Fig. 16**B and C). An analysis of the relationship between OHC voltage and OHC somatic forces showed that at frequencies above the transition, OHC forces would inject energy into the traveling wave. The resonant TM model and dual-traveling wave models, and likely other models, can produce an abrupt transition from non-amplifying to amplifying regions, similar to what was observed experimentally in **Fig. 16** (Lamb and Chadwick, 2014; Nankali et al., 2018; Dong and Olson, 2016).

The models in **Fig. 14** provide a mechanism for turning on the cochlear amplifier, but of equal interest is what turns the amplifier off at frequencies above the BF so the response will drop down. In most models, the peak comes down due to dissipation, but the mechanism for that dissipation is not certain. In the critical-layer absorption theory (Lighthill, 1981), the approach to local resonance slows the wave so much that a little bit of dissipation will bring down the response sharply. Fluid dissipation in the subtectorial space is included in many cochlear models (Allen, 1980; Prodanovic et al., 2015). TM thickness and porosity were shown to be significant in setting dissipation within the TM and the subtectorial space (Sellon et al., 2014, 2017). In cochleae lacking an organ of Corti (Eze and Olson, 2011) and in cochleae in which the TM was detached (Legan et al., 2000) the passive response peaked and then dropped off in the absence of a subtectorial space, so additional dissipative mechanisms exist. A recent model (Sasmal and Grosh, 2019) predicted that viscosity in the bulk fluid shapes apical responses while having little impact in basal and middle regions. However, in an experimental study the bulk fluid of perilymph could be made many times more viscous via perfusion with sodium hyaluronate (trademark Healon) solutions, without influencing cochlear mechanics as monitored with compound action potential (Wang and Olson, 2016). The perilymph perfusion would not have affected the endolymph, which is the fluid of the subtectorial space. Measurements of the mechanical impedance of the OCC in the gerbil base found it to be stiffness-dominated through at least 20 kHz, but experimental constraints prevented exploring the interesting BF and supra-BF frequency regions (Dong and Olson, 2009). de Boer and Nuttall's inverse calculation predicted that dissipation goes from negative in a region just basal to the BF-peak, and then becomes positive again (de Boer and Nuttall, 2000). There is still

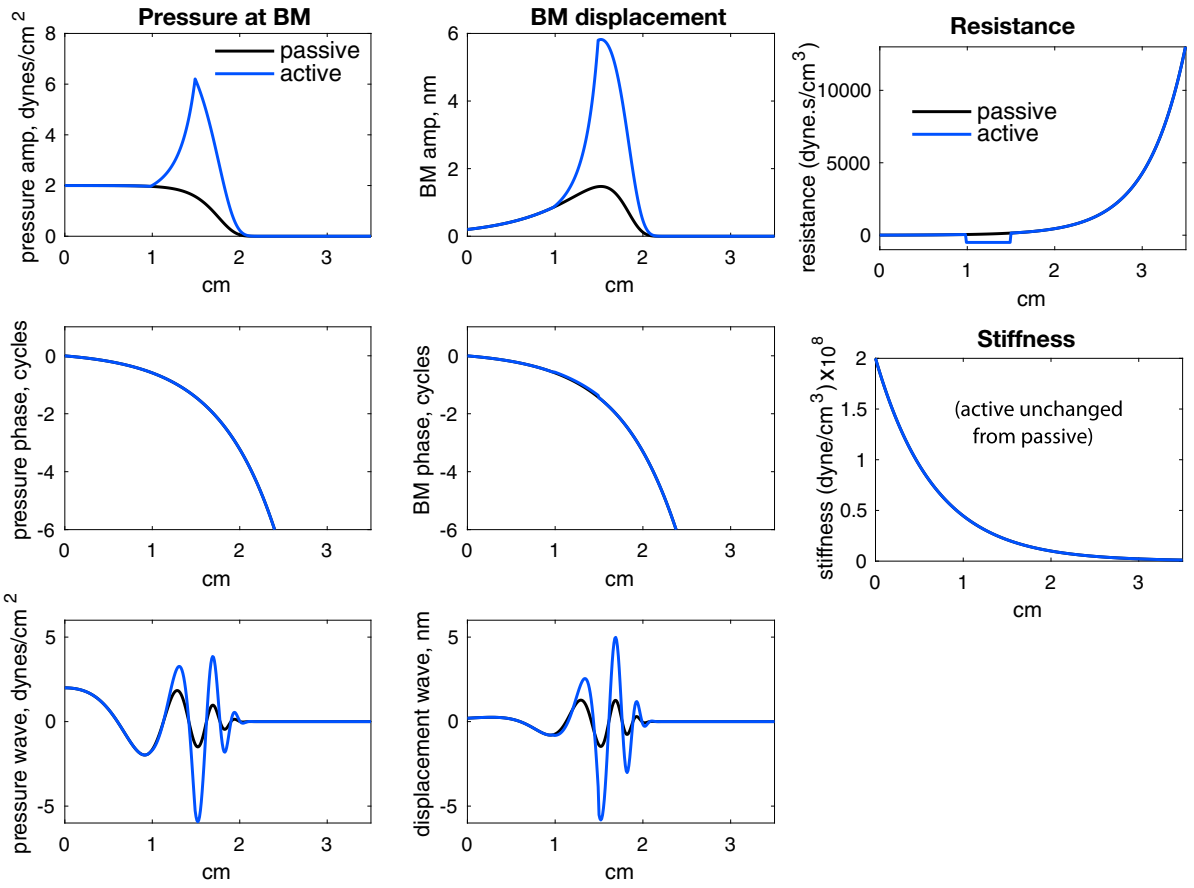

Figure 15 Amplification is incorporated into the computer model of **Fig. 8** by making the resistance negative over a small region just basal to the peak (resistance-versus location is plotted in third column). Black curves are the passive pressure and voltage responses to a 2 kHz stimulus (same as in **Fig. 8**) and blue are the active (amplified) responses.

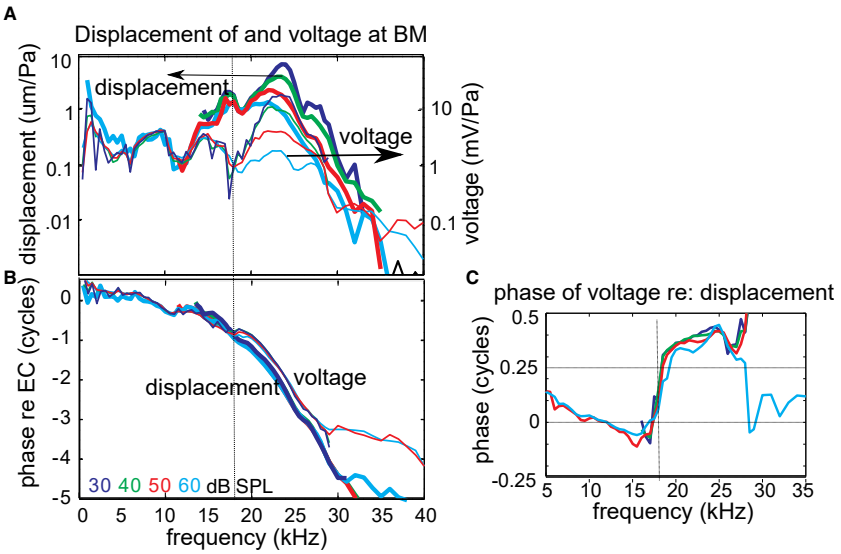

Figure 16 Simultaneous measurement of displacement of the BM and extracellular OHC voltage responses from a dual pressure/voltage sensor observed (A) Amplitudes that peaked at ~23 kHz at low SPL, (B) traveling wave phase accumulation that evinced the locality of the measurement and (C) a shift of voltage relative to displacement that indicates power input by OHC forcing at frequencies above the shift. Vertical line in all figures indicates the frequency where the BF nonlinearity begins and the phase shift occurs (Dong and Olson, 2013a).

Figure 17 A visual analogy. Left, the audible, highly resolved sounds a healthy ear hears. Middle, the diminished and poorly resolved sounds heard by an ear with sensorineural loss. Right, the hearing restored by a hearing aid, which improves volume but not fine resolution. The insets are cartoons of the traveling wave patterns in the cochlea when stimulated simultaneously by three tones, and underscore the visual analogy.

much to be sorted out regarding the frequency/place tuning of cochlear amplification, and alternative models to be considered (Cooper et al., 2018; vanderHeijden, 2014).

A fundamental property of the ear is that the frequency resolving mechanisms are located within the cochlea. The passive traveling wave provides rudimentary tuning, and OHC-based forces, working within the substrate of traveling wave and supporting cells and structures, provide a tremendous amount of additional frequency tuning. When OHC activity is lost due to acoustic damage or disease, there is no way to replace it with an external amplifier, like a standard hearing aid. Modern hearing aids contain sophisticated signal processors, but there is no way around the fact that after processing and amplifying the input signal, they send their output to the entire cochlea. **Fig. 17** is a visual analogy. As they age, many people will require a hearing aid, which will provide great benefit. However, they might be disappointed that while the hearing aid restores volume and some clarity, it does not restore natural hearing, because the resolving, "focusing" function of the ear operates locally, within the cochlea. A cochlear implant is a hearing aid that *does* operate locally, with an array of electrodes inserted into the cochlea. With further improvement in their spatial resolution, cochlear implants could potentially restore the local focusing of the sound stimulus that is so important in the natural ear (Senn et al., 2017; Wilson, 2017).

Some Additional Items of Import

Emissions

The discovery of sustained pressure fluctuations emerging from the ear as otoacoustic emissions (Kemp, 1978) reinforced the concept that the cochlea is mechanically active, and promised a noninvasive view to cochlear operation that could be used both in the laboratory (Kemp et al., 2008; Long et al., 2008) and clinically (Dalhoff et al., 2007; Abdala and Dhar, 2012; Janssen et al., 2008). Importantly, this noninvasive view could be used to probe cochlear mechanics in humans for which invasive measurements typically are not possible. Using emissions to probe cochlear mechanics is complicated by the cochlea's distributed mechanics, which leads to uncertainty about where in the cochlea an emission was generated, and the route the emission takes as it emerges from the cochlea (Dong and Olson, 2007; He et al., 2010; Siegel et al., 2005).

Interpreting emissions within the framework of the cochlear traveling wave has been a fruitful approach to their study (Shera and Guinan, 1999; Shera et al., 2008). For example, the steep phase-versus-frequency slope that is observed at the frequencies of the BF peak in intracochlear measurements in animals (**Fig. 9**) is manifested in a steeply-phased emission; the phase-versus frequency of the emission can in turn be used to indirectly and noninvasively observe the intracochlear phase-vs-frequency. Such reasoning, later combined with psychophysical measurements, has led to the finding that human tuning is sharper than that of most laboratory animals (Shera et al., 2010), see also (Joris et al., 2011). Some of the observations of otoacoustic emissions are not compatible with the wave-based theory (Siegel et al., 2005). Emissions are present in animals that do not have cochlear traveling waves (Bergevin et al., 2008), and in some cases oscillator models are appropriate for understanding their behavior (Bergevin et al., 2017).

Apical/Basal Differences

From auditory nerve recordings, it was known that there were differences in the the way the cochlear base and apex processed sound (Temchin et al., 2011; Kiang et al., 1986; Ohlemiller and Echteler, 1990). In **Fig. 18** auditory nerve tuning curves from gerbil show that the tuning is quite similar for fibers with CF above ~3 kHz (lower panels). These fibers show a steep cut-off at frequencies above the CF, and on the low-frequency side, an initial steep segment is followed by a low-frequency "tail" where the response threshold flattens out over a wide frequency range, particularly in **Fig. 18**E and F. As discussed in Section "**The Concept of Scaling Symmetry**" and **Fig. 5**, this similarity of tuning shape provided evidence for the concept of scaling symmetry. However, the tuning does not maintain this characteristic shape for fibers with CF below ~3 kHz (upper panels of **Fig. 18**). The two sides of the tuning curve are quite symmetrical in **Fig. 18**B (CF ~ 1 kHz), and in **Fig. 18**A, corresponding to fibers with CF of ~650 Hz, the low-frequency side cuts off more sharply than the high frequency side. The timing of auditory nerve responses also showed that apical

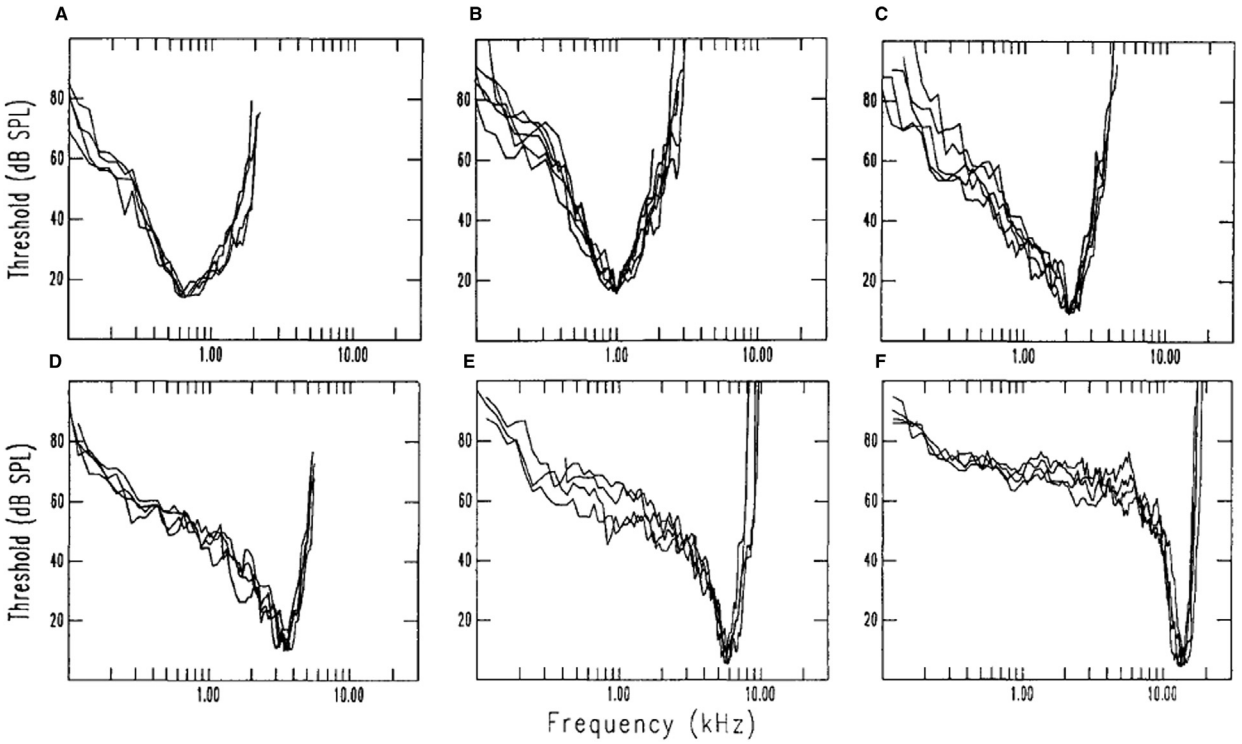

Figure 18 Auditory nerve tuning curves from gerbil show the quite similar tuning (evidence of scaling symmetry) at frequencies above ~3 kHz - lower panels, and less similar tuning at frequencies below ~3 kHz - upper panels (Ohlemiller and Echteler, 1990).

and basal processing differed, as was discussed with reference to glides in Section "**Back to the Traveling Wave**". Apical/basal differences have also been explored with cochlear emissions (Shera et al., 2010). In motion measurements, the new OCT-enabling ability to make measurements without opening the cochlear bone removes one of the major impediments to measurements from the apex. While the results from the mouse apex (**Fig. 13**) show many similarities to basal measurements (perhaps because the frequencies are still quite high in the mouse apex), in guinea pig and gerbil OCT-based measurements of apical responses show wide-band frequency tuning, or even low-pass tuning, with nonlinearity operating over a wide frequency range (Recio-Spinoso and Oghalai, 2017; Dong et al., 2018). In vitro preparations have also been used to explore the micromechanics in the apical region (Nowotny and Gummer, 2011; Warren et al., 2016).

Passive cochlear models (including the simple model in **Fig. 7**) naturally predict sharper tuning in the base than in the apex (Steele and Taber, 1979b), and a passive model incorporating the cochlea's snail-like curvature showed that curvature could enhance low frequency tuning (Manoussaki et al., 2006). Active models have explored apical processing, and predicted apical/basal response differences based on mechanisms that were either micromechanical (Reichenbach and Hudspeth, 2010), or a combination of micro and macromechanical (Sasmal and Grosh, 2019).

A recent paper focusing on human cochlear anatomy and motion responses included a set of micrographs from the base and apex of six species (Raufer et al., 2019) and **Fig. 19** shows this menagerie of cochlear anatomy. Of note are the width of the partition in the human apex (note scale bar in A), and the width to which the bony lamina extends, which can be right up to the inner pillar cell (all but human in the base) or further medial, not even close to the inner pillar (most pronounced in human and guinea pig in the apex). In human the fibrous attachment between the bone and the inner pillar forms a relatively compliant "bridge," which affects the passive motion responses in human temporal bone measurements (Raufer et al., 2019), and likely the active motion responses in live humans. The impact of the wide lamina on passive BM motion responses was explored in a cochlear model that contrasted primate and rodent anatomy (Taber and Steele, 1981). The images of **Fig. 19** reinforce that cochlear anatomy has basic similarity and also important variations across species and longitudinal location. On this point, even among humans, the cochlear length was found to vary from ~39 to 46 mm in 73 specimens (Erixon et al., 2009).

Efferent Effects

Cochlear responses are modulated by the brain by means of medial olivocochlear (MOC) efferent fibers that contact OHCs and lateral olivocochlear (LOC) efferents that contact auditory nerve fibers under IHCs (Guinan, 2006; Schofield, 2020). In animal studies, efferent stimulation changes cochlear emissions (Mountain, 1980), and reduces auditory nerve and BM responses (Stankovic and Guinan, 1999; Guinan and Cooper, 2008). The modulatory action of efferents is thought to improve signal detection

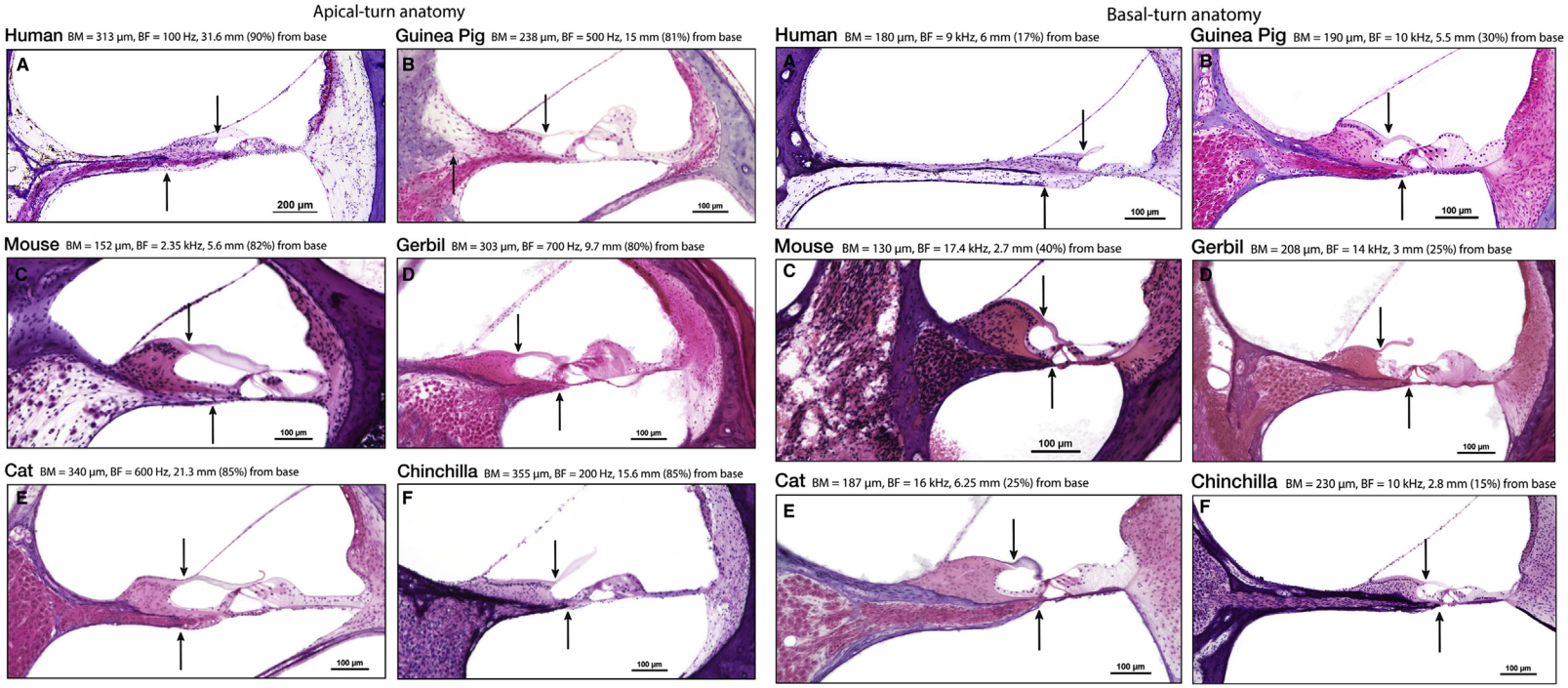

Figure 19 Apical (left set) and basal (right set) anatomy of several animals from the supplemental material of (Raufer et al., 2019). The up-arrow points to the most lateral extent of bone of the osseous spiral lamina and the down-arrow points to the attachment of TM to the limbus. These aspects of the anatomy were a focus of (Raufer et al., 2019).

in noise and offer some protection against acoustic trauma (Guinan, 2006; Sayles et al., 2017; Russell et al., 2008) and efferents are involved in the maintenance of neural circuitry (Yanbo et al., 2014). However, humans and animals who have had their olivocochlear bundle cut during surgery do not suffer from obvious hearing deficits (Scharf et al., 1997) and some mammalian species lack efferent projections to OHCs (Bruns and Schmieszek, 1980; Raphael et al., 1991). Thus, to first order the mature cochlea apparently does not need the brain to tell it what to do.

Summary

The understanding of the mechanical processing of the cochlea moves forward both steadily and in leaps brought on by technology, serendipity and the inspiration of individuals. The field of cochlear mechanics was greatly influenced by the introduction of the telephone, which brought engineers who needed to know what should be included in the acoustic signal of the phone, and today the explorers of cochlear mechanics are biologists, physiologists, neuroscientists, physical scientists and engineers. This article included some of the basic mathematics and analytical processing used in cochlear mechanics, to open the door to the rich quantitative literature on the cochlea.

The cochlea's special properties are its crystalline-like anatomy, its speed of operation to the 10s of microseconds, and its milli/micro/nano-scale mechanical traveling wave. The marvelous cell-based shaping and amplification of this wave, provided by the cochlear amplifier, gives rise to a highly frequency-resolved representation of the sound signal, which the brain then uses to hear. While much is understood about the mechanical processing of the cochlea, much remains unknown – about Prestin, about the role of the tectorial membrane, about mechanoelectric transduction and the electromechanical transduction that feeds back, and mainly, about how all these things work together to provide healthy cochlear operation. The "little mechanical brain" that is the mammalian cochlea is a unique and awe-inspiring organ.

Acknowledgments

I thank Christopher Shera, C. Elliott Strimbu, Yi Wang and Christina Vizcarra who commented on an early version of the chapter. I also thank those colleagues who sent me data and drawings for plotting and displaying.

References

Abdala, C., Dhar, S., 2012. Maturation and aging of the human cochlea: a view through the DPOAE looking glass. JARO 13, 403–421.
Adachi, M., Sugawara, M., Iwasi, K.H., 2000. Effect of turgor pressure on outer hair cell motility. J. Acoust. Soc. Am. 108, 2299–2306.
Allen, J.B., 1980. Cochlear micromechanics–A physical model of transduction. J. Acoust. Soc. Am. 68, 1660–1670.
Ashida, G., Carr, C.E., 2011. Sound localization: jeffress and beyond. Curr. Opin. Neurobiol. 21, 745–751.
Ashmore, J.F., 1987. A fast motile response in Guinea-pig outer hair cells: the cellular basis of the cochlear amplifier. J. Physiol. 388, 323–347.
Bartscha, T.F., Hengela, F.E., Oswalda, A., Dionnec, G., Chipendoa, I.V., Mangata, S.S., El Shatanofya, M., Shapiroc, L., Muller, U., Hudspeth, A.J., 2019. Elasticity of individual protocadherin 15 molecules implicates tip links as the gating springs for hearing. Proc. Natl. Acad. Sci. U. S. A. 116, 11048–11056.
Békésy, G., 1960. Experiments in Hearing. McGraw-Hill, New York.
Békésy, G., 1961. Concerning the pleasures of observing, and the mechanics of the inner ear. Nobel Lecture.
Bergevin, C., Freeman, D.M., Saunders, J.C., Shera, C.A., 2008. Otoacoustic emissions in humans, birds, lizards, and frogs: evidence for multiple generation mechanisms. J. Comp. Physiol. 194, 665–683.
Bergevin, C., Verhulst, S., vanDijk, P., 2017. Remote sensing the cochlea: otoacoustics. In: Manley, G., Gummer, A.W., Popper, A.N., Fay, R.R. (Eds.), Understanding the Cochlea, Springer Handbook of Auditory Research, vol. 62. Springer, Cham, pp. 287–318.
Beurg, M., Fettiplace, R., Nam, J.-H., Ricci, A.J., 2009. Localization of inner hair cell mechanotransducer channels using high-speed calcium imaging. Nat. Neurosci. 12, 553–558.
Brownell, W.E., Bader, C.R., Bertrand, D., DeRibaupierre, Y., 1985. Evoked mechanical responses of isolated cochlear outer hair cells. Science 227, 194–196.
Bruns, V., Schmieszek, E., 1980. Cochlear innervation in the greater horseshoe bat: demonstration of an acoustic fovea. Hear. Res. 3, 27–43.
Carney, L.H., McDuffy, M.J., Shekhter, I., 1999. Frequency glides in the impulse responses of auditory-nerve fibers. J. Acoust. Soc. Am. 105, 2384–2391.
Chadwick, R.S., Dimitriadis, E.K., Iwasa, K.H., 1996. Active control of waves in a cochlear model with subpartitions. Proc. Natl. Acad. Sci. U. S. A. 93, 2564–2569.
Chen, F., Zha, D., Fridberger, A., Zheng, J., Choudhury, N., Jacques, S.L., Wang, R.K., Shi, X., Nuttall, A.L., 2011. A differentially amplified motion in the ear for near-threshold sound detection. Nat. Neurosci. 14, 770–774.
Cody, A.R., Russell, I.J., 1987. The responses of hair cells in the basal turn of the guinea-pig cochlea to tones. J. Physiol. 383, 551–569.
Colburn, H.S., 1996. Computational models of binaural processing. In: Hawkins, H.L., McMullen, T.A., Popper, A.N., Fay, R.R. (Eds.), Auditory Computation, Springer Handbook of Auditory Research, vol. 6. Springer, NY, pp. 332–340.
Cooper, N.P., 1999. Radial variation in the vibrations of the cochlear partition. In: Wada, H., Takasaka, T.I.K., Ohyama, K., Koike, T. (Eds.), Proceedings of the International Symposium on Recent Developments in Auditory Mechanics, Sendai Japan. World Scientific Press, pp. 109–115.
Cooper, N.P., Vavakou, A., vanderHeijden, M., 2018. Vibration hotspots reveal longitudinal funneling of sound-evoked motion in the mammalian cochlea. Nat. Commun. 9, 3054 1–305412.
Corey, D.P., Maoiléidigh, D.Ó., Ashmore, J.F., 2017. Mechanical transduction processes in the hair cell. In: Manley, G., Gummer, A.W., Popper, A.N., Fay, R.R. (Eds.), Understanding the Cochlea, Springer Handbook of Auditory Research, vol. 62. Springer, Cham, pp. 75–111.
Cormack, J., Liu, Y., Nam, J.-H., Gracewski, S.M., 2015. Two-compartment passive frequency domain cochlea model allowing independent fluid coupling to the tectorial and basilar membranes. J. Acoust. Soc. Am. 137, 1117–1125.
Dalhoff, E., Turcanu, D., Zenner, H.-P., Gummer, A.W., 2007. Distortion product otoacoustic emissions measured as vibration on the eardrum of human subjects. Proc. Natl. Acad. Sci. U. S. A. 104, 1546–1551.
Dallos, P., 1986. Neurobiology of cochlear inner and outer hair cells: intracellular recordings. Hear. Res. 22, 185–198.

Dallos, P., Cheatham, M.A., 1971. Travel time in the cochlea and its determination from cochlear-microphonic data. J. Acoust. Soc. Am. 49, 1140–1143.
Dallos, P., Cheatham, M.A., Ferraro, J., 1974. Cochlear mechanics, nonlinearities and cochlear potentials. J. Acoust. Soc. Am. 55, 597–605.
de Boer, E., 1980. Auditory physics. Physical principles in hearing theory. I. Phys. Rep. 62, 87–174.
de Boer, E., 1984. Auditory physics. Physical principles in hearing theory. II. Phys. Rep. 105, 141–226.
De Boer, E., Nuttall, A.L., 1997. The mechanical waveform of the basilar membrane. I. frequency modulations ("glides") in impulse responses and cross-correlation functions. J. Acoust. Soc. Am. 101, 3583–3592.
de Boer, E., Nuttall, A.L., 2000. The mechanical waveform of the basilar membrane. III. Intensity effects. J. Acoust. Soc. Am. 107, 1497–1507.
deLaRochefoucauld, O., Olson, E.S., 2007. The role of organ of Corti mass in cochlear tuning. Biophys. J. 93, 3434–3450.
Delgutte, B., 1990. Two-tone rate suppression in auditory-nerve fibers: dependence on suppressor frequency and level. Hear. Res. 49, 225–246.
Dewey, J.B., Applegate, B.E., Oghalai, J.S., 2019. Amplification and suppression of traveling waves along the mouse organ of Corti: evidence for spatial variation in the longitudinal coupling of outer hair cell-generated forces. J. Neurosci. 39, 1805–1816.
Dong, W., Olson, E.S., 2007. Supporting evidence for reverse cochlear traveling waves. J. Acoust. Soc. Am. 123, 222–240.
Dong, W., Olson, E.S., 2009. In vivo impedance of the gerbil organ of Corti at auditory frequencies. Biophys. J. 97, 1233–1243.
Dong, W., Olson, E.S., 2013a. Detection of cochlear amplification and its activation. Biophys. J. 105, 1067–1078.
Dong, W., Olson, E.S., 2016. Two-tone suppression of simultaneous electrical and mechanical responses in the cochlea. Biophys. J. 111, 1805–1815.
Dong, W., Varavva, P., Olson, E.S., 2012. Sound transmission along the ossicular chain in common wild-type laboratory mice. Hear. Res. 301, 27–34.
Dong, W., Xia, A., Raphael, P.D., Puria, S., Applegate, B., Oghalai, J.S., 2018. Organ of Corti vibration within the intact gerbil cochlea measured by volumetric optical coherence tomography and vibrometry. J. Neurophysiol. 120, 2847–2857.
Duifhuis, H., 2012. Cochlear Mechanics: Introduction to a Time Domain Analysis of the Nonlinear Cochlea. Springer.
Eatock, R.A., Corey, D.P., Hudspeth, A.J., 1987. Adaptation of mechanoelectrical transduction in hair cells of the bullfrog's sacculus. J. Neurosci. 7, 2821–2836.
Edge, R.M., Evans, B.N., Pearce, M., Richter, C.P., Hu, X., Dallos, P., 1998. Morphology of the unfixed cochlea. Hear. Res. 124, 1–16.
Effertz, T., Scharr, A.L., Ricci, A.J., 2015. The how and why of identifying the hair cell mechano-electrical transduction channel. Pflugers Arch. 467, 73–84.
Eldredge, D.H., Miller, J.D., Bohne, B.A., 1981. A frequency-position map for the chinchilla cochlea. J. Acoust. Soc. Am. 69, 1091–1095.
Erixon, E., Högstorp, H., Wadin, K., Rask-Andersen, H., 2009. Variational anatomy of the human cochlea: implications for cochlear implantation. Otol. Neurotol. 30, 14–22.
Eze, N., Olson, E.S., 2011. Basilar membrane velocity in a cochlea with modified organ of Corti. Biophys. J. 100, 858–867.
Fahey, P.F., Allen, J.B., 1985. Nonlinear phenomena as observed in the ear canal and at the auditory nerve. J. Acoust. Soc. Am. 77, 599–612.
Fahey, P.F., Stagner, B.B., Lonsbury-Martin, B.L., Martin, G.K., 2000. Nonlinear interactions that could explain distortion product interference response areas. J. Acoust. Soc. Am. 108, 1786–1802.
Fallah, E., Strimbu, C.E., Olson, E.S., 2019. Nonlinearity and amplification in cochlear responses to single and multi-tone stimuli. Hear. Res. 377, 271–281.
Fettiplace, R., Kim, K.X., 2014. The physiology of mechanoelectrical transduction channels in hearing. Physiol. Rev. 94, 951–986.
Fisher, J.A.N., Nin, F., Reichenbach, T., Uthaiah, R.C., Hudsepth, A.J., 2012. The spatial pattern of cochlear amplification. Neuron 76, 989–997.
Fleischer, M., Schmidt, R., Gummer, A.W., 2010. Compliance profiles derived from a three-dimensional finite-element model of the basilar membrane. J. Acoust. Soc. Am. 127, 2973–2991.
Frank, G., Hemmert, W., Gummer, A.W., 1999. Limiting dynamics of high-frequency electromechanical transduction of outer hair cells. Proc. Natl. Acad. Sci. U. S. A. 96, 4420–4425.
Freeman, D.M., Abnet, C.C., Hemmert, W., Tsai, B.S., Weiss, T.F., 2003a. Dynamic material properties of the tectorial membrane: a summary. Hear. Res. 180, 1–10.
Freeman, D.M., Masaki, K., McAllister, A.R., Wei, J.L., Weiss, T.F., 2003b. Static material properties of the tectorial membrane: a summary. Hear. Res. 180, 11–27.
Fridberger, A., de Monvel, J.B., Zheng, J., Hu, N., Zou, Y., Ren, T., Nuttall, A., 2004. Organ of Corti potentials and the motion of the basilar membrane. J. Neurosci. 24, 10057–10063.
Gao, S.S., Raphael, P.D., Wang, R., Park, J., Xia, A., Applegate, B.E., Oghalai, J.S., 2013. In vivo vibrometry inside the apex of the mouse cochlea using spectral domain optical coherence tomography. Biomed. Opt. Express 4, 230–240.
Gavara, N., Chadwick, R.S., 2009. Collagen-based mechanical anisotropy of the tectorial membrane: implications for inter-row coupling of outer hair cell bundles. PLoS One 4, e4877.
Gavara, N., Chadwick, R.S., 2010. Noncontact microrheology at acoustic frequencies using frequency-modulated atomic force microscopy. Nat. Methods 7, 650–655.
Geisler, C.D., Nuttall, A.L., 1997. Two-tone suppression of basilar membrane vibrations in the base of the guinea pig cochlea using low-side suppressors. J. Acoust. Soc. Am. 102, 430–440.
Geisler, C.D., Yates, G.K., Patuzzi, R.B., Johnstone, B.M., 1990. Saturation of outer hair cell receptor currents causes two-tone suppression. Hear. Res. 44, 241–256.
Ghaffari, R., Aranyosi, A.J., Freeman, D.M., 2007. Longitudinally propagating traveling waves of the mammalian tectorial membrane. Proc. Natl. Acad. Sci. U. S. A. 104, 16510–16515.
Gold, T., Pumphrey, R.J., 1948. Hearing. I. The cochlea as a frequency analyzer. Proc. R. Soc. Lond. B Biol. Sci. 135, 462–491.
Greenwood, D.D., 1990. A cochlear frequency-position function for several species: 29 years later. J. Acoust. Soc. Am. 87, 2592–2605.
Grosh, K., Zheng, J., Zou, Y., de Boer, E., Nuttall, A.L., 2004. High-frequency electromotile responses in the cochlea. J. Acoust. Soc. Am. 115, 2178–2184.
Gueta, R., Barlam, D., Shneck, R., Rousso, I., 2008. Sound-evoked deflections of outer hair cells stereocilia arise from tectorial membrane anisotropy. Biophys. J. 94, 4570–4576.
Guinan, J.J., 2006. Olivocochlear efferents: anatomy, physiology, function, and the measurement of efferent effects in humans. Ear Hear. 27, 589–607.
Guinan, J.J., Cooper, N.P., 2008. Medial olivocochlear efferent inhibition of basilar-membrane responses to clicks: evidence for two modes of cochlear mechanical excitation. J. Acoust. Soc. Am. 124, 1080–1092.
Gummer, A.W., Dong, W., Ghaffari, R., Freeman, D.M., 2017. Electromechanical feedback mechanisms and power transfer in the mammalian cochlea. In: Manley, G., Gummer, A.W., Popper, A.N., Fay, R.R. (Eds.), Understanding the Cochlea, Springer Handbook of Auditory Research, vol. 62. Springer, Cham, pp. 147–181.
Hackney, C.M., Furness, D.M., 2013. The composition and role of cross links in mechanoelectrical transduction in vertebrate sensory hair cells. J. Cell Sci. 126, 1721–1731.
He, W., Fridberger, A., Porsov, E., Ren, T., 2010. Fast reverse propagation of sound in the living cochlea. Biophys. J. 98, 2497–2505.
Helmholtz, H.L.F., 1885. On the Sensations of Tone. Dover, New York.
Hong, S.S., Freeman, D.M., 2006. Doppler optical coherence microscopy for studies of cochlear mechanics. J. Biomed. Optic. 11, 054014.
Howard, J., Hudspeth, A.J., 1988. Compliance of the hair bundle associated with gating of mechanoelectrical transduction channels in the bullfrog's saccular hair cell. Neuron 1, 189–199.
Hubbard, A., 1993. A traveling-wave amplifier model of the cochlea. Science 259, 68–71.
Hudspeth, A.J., 1982. Extracellular current flow and the site of transduction by vertebrate hair cells. J. Neurosci. 2, 1–10.
Iwasa, K.H., 2001. A two-state piezoelectric model for outer hair cell. Motility Biophys. J. 81, 2495–2506.
Iwasa, K.H., 2018. Energy output from a single outer hair cell. Biophys. J. 111, 2500–2511.
Iwasa, K.H., Adachi, M., 1997. Force generation in the outer hair cell of the cochlea. Biophys. J. 73, 546–555.
Jacques, S.L., Ramamoorthy, S., Petrie, T.C., Nguyen-Huynh, A., AL Nuttall, 2013. A concise algorithm for detection of vibration from Fourier domain OCT. Proc. SPIE 8565 85652B. Photonic Therapeutics and Diagnostics IX.
Janssen, T.J., Muller, J., 2008. Otoacoustic Emissions as a diagnostic tool in a clinical context. In: Manley, G.A., Fay, R.R., Popper, A.N. (Eds.), Active Processes and Otoacoustic Emissions in Hearing, Springer Handbook of Auditory Research, vol. 30. Springer, NY, pp. 421–460.

Johnson, S.L., Beurg, M., Marcotti, W., Fettiplace, R., 2011. Prestin-driven cochlear amplification is not limited by the outer hair cell membrane time constant. Neuron 70, 1143–1154.
Joris, P.X., Bergevin, C., Kalluri, R., McLaughlin, M., Michelet, P., vanderHeijden, M., Shera, C.A., 2011. Frequency selectivity in Old-World monkeys corroborates sharp cochlear tuning in humans. Proc. Natl. Acad. Sci. U. S. A. 108, 17516–17520.
Kachar, B., Parakkal, M., Kurc, M., Zhao, Y., Gillespie, P.G., 2000. High-resolution structure of hair-cell tip links. Proc. Natl. Acad. Sci. U. S. A. 97, 13336–13341.
Kale, S., Olson, E.S., 2015. Intracochlear scala media pressure: measurement, analysis and implications for models of cochlear mechanics. Biophys. J. 109, 2678–2688.
Kapuria1, S., Steele, C.R., Puria, S., 2017. Unraveling the mystery of hearing in gerbil and other rodents with an arch-beam model of the basilar membrane. Sci. Rep. 7, 228.
Karavitaki, K.D., Corey, D.P., 2010. Sliding adhesion confers coherent motion to hair cell stereocilia and parallel gating to transduction channels. J. Neurosci. 30, 9051–9063.
Karavitaki, K.D., Mountain, D.C., 2007. Evidence for outer hair cell driven oscillatory fluid flow in the tunnel of Corti. Biophys. J. 92, 3284–3293.
Kazmierczak, P., Sakaguchi, H., Tokita, J., Wilson-Kubalek, E.M., Milligan, R.A., Müller, U., Kachar, B., 2007. Cadherin 23 and protocadherin 15 interact to form tip-link filaments in sensory hair cells. Nature 449, 87–91.
Kemp, D.T., 1978. Stimulated acoustic emissions from within the human auditory system. J. Acoust. Soc. Am. 64, 1386–1391.
Kemp, D.T., 2008. Otoacoustic emissions: concepts and origins. In: Manley, G.A., Fay, R.R., Popper, A.N. (Eds.), Active Processes and Otoacoustic Emissions in Hearing, Springer Handbook of Auditory Research, vol. 30. Springer, NY, pp. 1–38.
Kennedy, H.J., Crawford, A.C., Fettiplace, R., 2005. Force generation by mammalian hair bundles supports a role in cochlear amplification. Nature 433, 880–883.
Kiang, N.Y.S., Liberman, M.C., Sewell, W.F., Guinan, J.G., 1986. Single unit clues to cochlear mechanisms. Hear. Res. 22, 171–182.
Kirk, D.L., Moleirinho, A., Patuzzi, R.B., 1997. Microphonic and DPOAE measurements suggest a micromechanical mechanism for the 'bounce' phenomenon following low-frequency tones. Hear. Res. 112, 69–86.
Kolston, P.J., 2000. The importance of phase data and model dimensionality to cochlear mechanics. Hear. Res. 145, 25–36.
Lamb, J.S., Chadwick, R.S., 2011. Dual traveling waves in an inner ear model with two degrees of freedom. Phys. Rev. Lett. 107, 088101.
Lamb, J.S., Chadwick, R.S., 2014. Phase of shear vibrations within cochlear partition leads to activation of the cochlear amplifier. PLoS One 9, e85969 1–7.
Lee, H.Y., Raphael, P.D., Xia, A., Kim, J., Grillet, N., Park, J., Applegate, B.E., Ellerbee-Bowden, A.K., Oghalai, J.S., 2016. Two-dimensional cochlear micromechanics measured *in vivo* demonstrate radial tuning within the mouse organ of Corti. J. Neurosci. 36, 8160–8173.
Legan, P.K., Lukashkina, V.A., Goodyear, R.J., Kössi, M., Russell, I.J., Richardson, G.P., 2000. A targeted deletion in alphatectorin reveals that the tectorial membrane is required for the gain and timing of cochlear feedback. Neuron 28, 273–285.
Lemons, C., Sellon, J.B., Boatti, E., Filizzola, D., Freeman, D.M., Meaud, J., 2019. Anisotropic material properties of wild-type and *Tectb*$^{-/-}$ tectorial membranes. Biophys. J. 116, 573–585.
Lighthill, J., 1981. Energy flow in the cochlea. J. Fluid Mech. 106, 149–213.
Lim, D.J., 1980. Cochlear anatomy related to cochlear micromechanics. A review. J. Acoust. Soc. Am. 67 (5), 1686–1695.
Lim, D.J., 1986. Functional structure of the organ of Corti: a review. Hear. Res. 22, 117–146.
Lin, N.C., Strimbu, C.E., Hendon, C.P., Olson, E.S., 2017a. Adapting a commercial spectral domain optical coherence tomography system for time-locked displacement and electrophysiological measurements. In: Bergevin, C., Puria, S. (Eds.), Proceedings of the Mechanics of Hearing Meeting, Ontario Canada. AIP Press, p. 080004.
Lin, N.C., Hendon, C.P., Olson, E.S., 2017b. Signal competition in optical coherence tomography and its relevance for cochlear vibrometry. J. Acoust. Soc. Am. 141, 395–405.
Liu, W., Atturo, F., Aldaya, R., Santi, P., Cureoglu, S., Obwegeser, S., Glueckert, R., Pfaller, K., Schrott-Fischer, A., Rask-Andersen, H., 2015a. Macromolecular organization and fine structure of the human basilar membrane - relevance for cochlear implantation. Cell Tissue Res. 360, 245–262.
Liu, Y., Gracewski, S.M., Nam, J.-H., 2015b. Consequences of location-dependent organ of Corti micro-mechanics. PLoS One 10, e0133284.
Long, G.R., Talmadge, C.L., Lee, J., 2008. Measuring distortion product otoacoustic emissions using continuously sweeping primaries. J. Acoust. Soc. Am. 124, 1613–1626.
Lumpkin, E.A., Hudspeth, A.J., 1995. Detection of Ca^{+2} entry through mechanosensitive channels localizes the site of mechanoelectrical transduction in hair cells. Proc. Natl. Acad. Sci. U. S. A. 92, 10297–10301.
Manoussaki, D., Dimitriadis, E.K., Chadwick, R.S., 2006. Cochlea's graded curvature effect on low frequency waves. Phys. Rev. Lett. 96, 088701 1–4.
Martin, P., Bozovic, D., Choe, Y., Hudspeth, A.J., 2003. Spontaneous oscillation by hair bundles of the bullfrog's sacculus. J. Neurosci. 23, 4533–4548.
Meaud, J., Grosh, K., 2011. Coupling active hair bundle mechanics, fast adaptation, and somatic motility in a Cochlear model. Biophys. J. 100, 2576–2585.
Meaud, J., Grosh, K., 2012. Response to a pure tone in a nonlinear mechanical-electrical-acoustical model of the cochlea. Biophys. J. 102, 1237–1246.
Mellado Lagarde, M.M., Drexl, M., Lukashkina, V.A., Lukashkin, A.N., Russell, I.J., 2008. Outer hair cell somatic, not hair bundle, motility is the basis of the cochlear amplifier. Nat. Neurosci. 11, 746–748.
Motallebzadeh, H., Soons, J.A.M., Puria, S., 2018. Cochlear amplification and tuning depend on the cellular arrangement within the organ of Corti. Proc. Natl. Acad. Sci. U. S. A. 115, 5762–5767.
Mountain, D.C., 1980. Changes in endolymphatic potential and crossed olivocochlear bundle stimulation alter cochlear mechanics. Science 210, 71–72.
Naidu, R.C., Mountain, D.C., 1998. Measurements of the stiffness map challenge a basic tenet of cochlear theories. Hear. Res. 124, 124–131.
Nakajima, H.H., Dong, W., Olson, E.S., Merchant, S.N., Ravicz, M.E., Rosowski, J.J., 2008. Differential intracochlear sound pressure measurements in normal human temporal bones. J. Assoc. Res. Otolaryngol. 10, 23–26.
Nankali, A., Wang, Y., Olson, E.S., Grosh, K., 2018. Frequency structure in intracochlear voltage supports the concept of tectorial membrane mechanical resonance. AIP Conf. Proc. 1965, 040002-1–040002-6 https://doi.org/10.1063/1.5038462.
Naryan, S.S., Temchin, A.N., Recio, A., Ruggero, M.A., 1998. Frequency tuning of basilar membrane and auditory nerve fibers in the same cochleae. Science 282, 1882–1884.
Neely, S.T., Kim, D.O., 1986. A model for active elements in cochlear biomechanics. J. Acoust. Soc. Am. 79, 1472–1480.
Nowotny, M., Gummer, A.W., 2011. Vibration responses of the organ of Corti and the tectorial membrane to electrical stimulation. J. Acoust. Soc. Am. 130, 3852–3872.
Ohlemiller, K.K., Echteler, S.M., 1990. Functional correlates of characteristic frequency in single cochlear nerve fibers of the Mongolian gerbil. J. Comp. Physiol. 167, 329–338.
Olson, E.S., 1998. Observing middle and inner ear mechanics with novel intracochlear pressure sensors. J. Acoust. Soc. Am. 103, 3445–3463.
Olson, E.S., 1999. Direct measurement of intracochlear pressure waves. Nature 402, 526–529.
Olson, E.S., 2001. Intracochlear pressure measurements related to cochlear frequency tuning. J. Acoust. Soc. Am. 110, 349–367.
Olson, E.S., 2013. Fast waves, slow waves and cochlear excitation. J. Acoust. Soc. Am. 133, 3508.
Olson, E.S., Mountain, D.C., 1994. Mapping the cochlear partition's stiffness to its cellular architecture. J. Acoust. Soc. Am. 95, 395–400.
Olson, E.S., Duifhuis, D., Steele, C.R., 2012. von Békésy and cochlear mechanics. Hear. Res. 293, 31–43.
OMaoileidigh, D., Julicher, F., 2010. The interplay between active hair bundle motility and electromotility in the cochlea. J. Acoust. Soc. Am. 128, 1175–1190.
Oroz, J., Galera-Prat, A., Hervás, R., Valbuena, A., Fernández-Bravo, D., Carrión-Vázquez, M., 2019. Nanomechanics of tip-link cadherins. Sci. Rep. 9, 13306.
Pan, B., Géléoc, G.S., Asai, Y., Horwitz, G.C., Kurima, K., Ishikawa, K., Kawashima, Y., Griffith, A.J., Holt, J.R., 2013. TMC1 and TMC2 are components of the mechanotransduction channel in hair cells of the mammalian inner ear. Neuron 79, 504–515.
Pecka, M., 2020. Coding of Spatial Information. Chapter in this Publication, in press.
Peterson, L.C., Bogert, B.P., 1950. A dynamical theory of the cochlea. J. Acoust. Soc. Am. 22, 369–381.
Pickles, J.O., Comis, S.D., Osborne, M.P., 1984. Cross-links between stereocilia in the guinea pig organ of Corti, and their possible relation to sensory transduction. Hear. Res. 15, 103–112.
Plassman, W., Peetz, W., Schmidt, M., 1987. The cochlea in gerbilline rodents. Brain Behav. Evol. 30, 82–101.

Prodanovic, S., Gracewski, S., Nam, J.-H., 2015. Power dissipation in the subtectorial space of the mammalian cochlea is modulated by inner hair cell stereocilia. Biophys. J. 108, 479–488.
Pujol, R., Lenoir, M., Ladrech, S., Tribillac, F., Rebillard, G., 1991. Correlation within and across species between the length of outer hair cells and the frequency coding of the cochlea. In: Cazals, Demany, Horner (Eds.), Auditory Physiology and Perception. Pergamon Press, pp. 45–52.
Rabbitt, R.D., Clifford, S., Breneman, K.D., Farrell, B., Brownell, W.E., 2019. Power efficiency of outer hair cell somatic electromotility. PLoS Comput. Biol. 5, e1000444.
Ramamoorthy, S., Deo, N.V., Grosh, K., 2007. A mechano-electro-acoustical model for the cochlea: response to acoustic stimuli. J. Acoust. Soc. Am. 121, 2758–2773.
Raphael, Y., Lenoir, M., Wroblewski, R., Pujol, R., 1991. The sensory epithelium and its innervation in the mole rat cochlea. J. Comp. Neurol. 314, 367–382.
Raufer, S., Guinan Jr., J.J., Nakajima, H.H., 2019. Cochlear partition anatomy and motion in humans differ from the classic view of mammals. Proc. Natl. Acad. Sci. U. S. A. 116, 13977–13982.
Recio, A., Rich, N.C., Narayan, S., Ruggero, M.A., 1998. Basilar-membrane responses to clicks at the base of the chinchilla cochlea. J. Acoust. Soc. Am. 103, 1972–1989.
Recio-Spinoso, A., Oghalai, J.S., 2017. Mechanical tuning and amplification within the apex of the guinea pig cochlea. J. Physiol. 595, 4549–4561.
Reichenbach, T., Hudspeth, A.J., 2010. A ratchet mechanism for amplification in low-frequency mammalian hearing. Proc. Natl. Acad. Sci. U. S. A. 107, 4973–4978.
Reichenbach, T., Hudspeth, A.J., 2014. The physics of hearing: fluid mechanics and the active process of the inner ear. Rep. Prog. Phys. 77, 1–45.
Ren, T., 2002. Longitudinal pattern of basilar membrane vibration in the sensitive cochlea. Proc. Natl. Acad. Sci. U. S. A. 99, 17101–17106.
Rhode, W.S., 1971. Observations on the vibration of the basilar membrane in squirrel monkey using the Mossbauer technique. J. Acoust. Soc. Am. 49, 1218–1231.
Rhode, W.S., 2007a. Basilar membrane mechanics in the 6–9 kHz region of sensitive chinchilla cochleae. J. Acoust. Soc. Am. 121, 2792–2804.
Rhode, W.S., 2007b. Mutual suppression in the 6 kHz region of sensitive chinchilla cochleae. J. Acoust. Soc. Am. 121, 2805–2818.
Ricci, A.J., Crawford, A.C., Fettiplace, R., 2000. Active hair bundle motion linked to fast transducer adaptation in auditory hair cells. J. Neurosci. 20, 7131–7142.
Richardson, G.P., Lukashkin, A.N., Russell, I.J., 2008. The tectorial membrane: one slice of a complex cochlear sandwich. Curr. Opin. Otolaryngol. Head Neck Surg. 16, 458–464.
Richter, C.-P., Emadi, G., Getnick, G., Quesnel, A., Dallos, P., 2007. Tectorial membrane stiffness gradients. Biophys. J. 93, 2265–2276.
Robles, L., Ruggero, M.A., 2001. Mechanics of the mammalian cochlea. Physiol. Rev. 81, 1305–1352.
Ruben, R., 2020. The developing concept of tonotopic organization of the inner ear. J. Assoc. Res. Otolaryngol. 21, 1–20.
Russell, I.J., Legan, P.K., Lukashkina, V.A., Lukashkin, A.N., Goodyear, R.J., Richardson, G.P., 2007. Sharpened cochlear tuning in a mouse with a genetically modified tectorial membrane. Nat. Neurosci. 10, 215–223.
Russell, I.J., AN, L., 2008. Cellular and molecular mechanisms in the efferent control of cochlear nonlinearities. In: Manley, G.A., Fay, R.R., Popper, A.N. (Eds.), Active Processes and Otoacoustic Emissions in Hearing, Springer Handbook of Auditory Research, vol. 30. Springer, NY, pp. 343–379.
Sachs, M.B., Kiang, N.Y.S., 1968. Two-tone inhibition in auditory nerve fibers. J. Acoust. Soc. Am. 43, 1120–1128.
Salt, A.N., Brown, D.J., Hartsock, J.H., Plontke, S.K., 2009. Displacements of the organ of Corti by gel injections into the cochlear apex. Hear. Res. 250, 63–75.
Santos-Sacchi, J., 1993. Harmonics of outer hair cell motility. Biophys. J. 65, 2217–2227.
Santos-Sacchi, J., Tan, W., 2018. The frequency response of outer hair cell voltage-dependent motility is limited by kinetics of Prestin. J. Neurosci. 38, 5495–5506.
Santos-Sacchi, J., Song, L., Zheng, J., Nuttall, A.L., 2006. Control of mammalian cochlear amplification by chloride anions. J. Neurosci. 26, 3992–3998.
Santos-Sacchi, J., Navaratnam, D., Raphael, R., Oliver, D., 2017. Prestin–molecular mechanisms underlying outer hair cell electromotility. In: Manley, G., Gummer, A.W., Popper, A.N., Fay, R.R. (Eds.), Understanding the Cochlea, Springer Handbook of Auditory Research, vol. 62. Springer, Cham, pp. 113–145.
Sasmal, A., Grosh, K., 2019. Unified cochlear model for low- and high-frequency mammalian hearing. Proc. Natl. Acad. Sci. U. S. A. 116, 13983–13988.
Sayles, M., Heinz, M.G., 2017. Afferent coding and efferent control in the normal and impaired cochlea. In: Manley, G., Gummer, A.W., Popper, A.N., Fay, R.R. (Eds.), Understanding the Cochlea, Springer Handbook of Auditory Research, vol. 62. Springer, Cham, pp. 215–252.
Scharf, B., Magnan, J., Chays, A., 1997. On the role of the olivocochlear bundle in hearing: 16 case studies. Hear. Res. 103, 101–122.
Schmiedt, R.A., Zwislocki, J.J., 1977. Comparison of sound-transmission and cochlear-microphonic characteristics in Mongolian gerbil and guinea pig. J. Acoust. Soc. Am. 61, 133–149.
Schofield, B., 2020. The Efferent System in the Cochlea. Chapter in this Publication, in press.
Sellon, J.B., Ghaffari, R., Farrahi, S., Richardson, G.P., Freeman, D.M., 2014. Porosity controls spread of excitation in tectorial membrane traveling waves. Biophys. J. 106, 1406–1413.
Sellon, J.B., Ghaffari, R., Freeman, D.M., 2017. Geometric requirements for tectorial membrane traveling waves in the presence of cochlear loads. Biophys. J. 112, 1059–1062.
Senn, P., Roccio, M., Hahnewald, S., Frick, C., Kwiatkowska, M., Ishikawa, M., Bako, P., Li, H., Edin, F., Liu, W., Rask-Andersen, H., Pyykko, I., Zou, J., Mannerstrom, M., Keppner, H., Homsy, A., Laux, E., Llera, M., Lellouche, J.-P., Ostrovsky, S., Banin, E., Gedanken, A., Perkas, N., Wank, U., Wiesmuller, K.-H., Mistrik, P., Benav, H., Garnham, C., Jolly, C., Gander, F., Ulrich, P., Muller, M., Lowenheim, H., 2017. NANOCI - nanotechnology based cochlear implant with gapless interface to auditory neurons. Otol. Neurotol. 38, e224–e231.
Shera, C.A., 2001a. Frequency glides in click responses of the basilar membrane and auditory nerve: their scaling behavior and origin in traveling-wave dispersion. J. Acoust. Soc. Am. 109, 2023–2034.
Shera, C.A., 2001b. Intensity-invariance of fine time structure in basilar membrane click responses: implications for cochlear mechanics. J. Acoust. Soc. Am. 110, 332–348.
Shera, C.A., Guinan Jr., J.J., 1999. Evoked otoacoustic emissions arise by two fundamentally different mechanisms: a taxonomy for mammalian OAEs. J. Acoust. Soc. Am. 105, 798.
Shera, C.A., Guinan Jr., J.J., 2008. Mechanisms of mammalian otoacoustic emission. In: Manley, G.A., Fay, R.R., Popper, A.N. (Eds.), Active Processes and Otoacoustic Emissions in Hearing, Springer Handbook of Auditory Research, vol. 30. Springer, NY, pp. 305–342.
Shera, C.A., Guinan Jr., J.J., Oxenham, A.J., 2010. Otoacoustic estimation of cochlear tuning: validation in the chinchilla. J. Assoc. Res. Otolaryngol. 11, 343–365.
Shuping, J., He, D.Z.Z., 2005. Motility-associated hair-bundle motion in mammalian outer hair cells. Nat. Neurosci. 8, 1028–1034.
Siebert, W.M., 1974. Ranke revisited–a simple short-wave cochlear model. J. Acoust. Soc. Am. 56, 594–600.
Siegel, J.H., Cerka, A.J., Recio-Spinoso, A., Temchin, A.N., vanDijk, P., Ruggero, M.A., 2005. Delays of stimulus-frequency otoacoustic emissions and cochlear vibrations contradict the theory of coherent reflection filtering. J. Acoust. Soc. Am. 118, 2434–2443.
Sirjani, D.B., Salt, A.N., Gill, R.M., Hale, S.A., 2003. The influence of transducer operating point on distortion generation in the cochlea. J. Acoust. Soc. Am. 115.
Soons, J.A.M., Ricci, A.J., Steele, C.R., Puria, S., 2015. Cytoarchitecture of the mouse organ of Corti from base to apex, determined using in situ two-photon imaging. J. Assoc. Res. Otolaryngol. 16, 47–66.
Sotomayor, M., Weihofen, W.A., Gaudet, R., Corey, D.P., 2012. Structure of a force-conveying cadherin bond essential for inner-ear mechanotransduction. Nature 492, 128–132.
Stankovic, K.M., Guinan, J.J., 1999. Medial efferent effects on auditory-nerve responses to tail-frequency tones. I. Rate reduction. J. Acoust. Soc. Am. 106, 857–869.
Steele, C.R., Taber, L.A., 1979a. Comparison of WKB calculations and experimental results for three-dimensional cochlear models. J. Acoust. Soc. Am. 60, 1007–1018.
Steele, C.R., Taber, L.A., 1979b. Comparison of WKB and finite difference calculations for a two-dimensional cochlear model. J. Acoust. Soc. Am. 65, 1001–1006.
Strimbu, C.E., Prasada, S., Hakizimana, P., Fridberger, A., 2019. Control of hearing sensitivity by tectorial membrane calcium. Proc. Natl. Acad. Sci. U. S. A. 116, 5756–5764.
Taber, L.A., Steele, C.R., 1981. Cochlear model including three-dimensional fluid and four modes of partition flexibility. J. Acoust. Soc. Am. 70, 426–436.
Temchin, A.N., Rich, N.C., Ruggero, M.A., 2008. Threshold tuning curves of chinchilla auditory-nerve fibers. I. Dependence on characteristic frequency and relation to the magnitudes of cochlear vibrations. J. Neurophysiol. 100, 2889–2898.
Temchin, A.N., Recio-Spinoso, A., Ruggero, M.A., 2011. Timing of cochlear responses inferred from frequency-threshold tuning curves of auditory-nerve fibers. Hear. Res. 272, 178–186.
vanderHeijden, M., 2014. Frequency selectivity without resonance in a fluid waveguide. Proc. Natl. Acad. Sci. U. S. A. 111, 14548–14552.

Velez-Ortega, A.C., Frolenkov, G.I., 2019. Building and repairing the stereocilia cytoskeleton in mammalian auditory hair cells. Hear. Res. 376, 47–67.
Verschooten, E., Shamma, S., Oxenham, A.J., Moore, B.C.J., Joris, P.X., Heinz, M.G., Plack, C.J., 2019. The upper frequency limit for use of phase locking to code temporal fine structure in humans: a compilation of viewpoints. Hear. Res. 377, 109–121.
Versteegh, C.P., vanderHeijden, M., 2013. The spatial buildup of compression and suppression in the mammalian cochlea. JARO 14, 523–545.
Wang, R.K., Nuttall, A.L., 2010. Phase sensitive optical coherence tomography imaging of the tissue motion within the organ of Corti at a subnanometer scale: a preliminary study. J. Biomed. Optic. 15, 056005.
Wang, Y., Olson, E.S., 2016. Cochlear perfusion with a viscous fluid. Hear. Res. 337, 1–11.
Wang, Y., Fallah, E., Olson, E.S., 2019. Adaptation of cochlear amplification to low endocochlear potential. Biophys. J. 116, 1769–1786.
Warren, R.L., Ramamoorthy, S., Ciganović, N., Zhang, Y., Wilson, T.M., Petrie, T., Wang, R.K., Jacques, S.L., Reichenbach, T., Nuttall, A.L., Fridberger, A., 2016. Minimal basilar membrane motion in low-frequency hearing. Proc. Natl. Acad. Sci. U. S. A. 113, E4304–E4310.
Wegel, R.L., Lane, C.E., 1924. The auditory masking of one pure tone by another and its probable relation to the dynamics of the inner ear. Phys. Rev. 23, 266–285.
Weiss, T.F., Freeman, D.M., 1997. Equilibrium behavior of an isotropic polyelectrolyte gel model of the tectorial membrane: the role of fixed charges. Int. J. Oper. Res. 3, 351–361.
West, C.D., 1985. The relationship of the spiral turns of the cochlea and the length of the basilar membrane to the range of audible frequencies in ground dwelling mammals. J. Acoust. Soc. Am. 77, 1091–1101.
Wever, E.G., 1962. Development of traveling-wave theories. J. Acoust. Soc. Am. 34, 1319–1324.
Wilson, B.S., 2017. The cochlear implant and possibilities for narrowing the remaining gaps between prosthetic and normal hearing. World J. Otorhinolaryngol. Head Neck Surg. 3, 200–210.
Yanbo, Y., Liberman, L.D., Maison, S.F., Liberman, M.C., 2014. Olivocochlear innervation maintains the normal modiolar-pillar and habenular-cuticular gradients in cochlear synaptic morphology. J. Assoc. Res Otolaryngol. 15, 571–583.
Yoon, Y.-J., Steele, C.R., Puria, S., 2011. Feed-forward and feed-backward amplification model from cochlear cytoarchitecture: an interspecies comparison. Biophys. J. 100, 1–10.
Zheng, J., Shen, W., He, D.Z., Long, K.B., Madison, L.D., Dallos, P., 2000. Prestin in the motor protein of cochlear outer hair cells. Nature 405, 149–155.
Zhou, W., Nam, J.-H., 2019. Probing hair cell's mechanotransduction using two-tone suppression measurements. Sci. Rep. 9, 4626.
Zweig, G., 1991. Finding the impedance of the organ of Corti. J. Acoust. Soc. Am. 89, 1229–1254.
Zwislocki, J.J., 1986. Analysis of cochlear mechanics. Hear. Res. 22, 155–169.